

Ahmad Arnous | Martin Zeckra | Agostina Venerdini |
Patricia Alvarado | Ramón Arrowsmith | Julien Guillemoteau |
Angela Landgraf | Antonio Gutiérrez | Manfred R. Strecker

Neotectonic Activity in the Low-Strain Broken Foreland (Santa Bárbara System) of the North-Western Argentinean Andes (26°S)

Suggested citation referring to the original publication:

Lithosphere 2020 (2020) 1, 1–25

DOI <https://doi.org/10.2113/2020/8888588>

ISSN (print) 1941-8264

ISSN (online) 1947-4253

Postprint archived at the Institutional Repository of the Potsdam University in:

Postprints der Universität Potsdam

Mathematisch-Naturwissenschaftliche Reihe ; 1008


ISSN 1866-8372

<https://nbn-resolving.org/urn:nbn:de:kobv:517-opus4-480183>

DOI <https://doi.org/10.25932/publishup-48018>

Research Article

Neotectonic Activity in the Low-Strain Broken Foreland (Santa Bárbara System) of the North-Western Argentinean Andes (26°S)

Ahmad Arnous ^{1,2}, Martin Zeckra,¹ Agostina Venerdini,^{3,4} Patricia Alvarado,^{3,4} Ramón Arrowsmith,⁵ Julien Guillemoteau,¹ Angela Landgraf,¹ Antonio Gutiérrez,² and Manfred R. Strecker¹

¹Institute of Geosciences, University of Potsdam, Potsdam, Germany

²Instituto Miguel Lillo (Departamento de Ciencias Naturales e Instituto Miguel Lillo), Universidad Nacional de Tucumán, Tucumán, Argentina

³Centro de Investigaciones de la Geósfera y Biósfera, Consejo Nacional de Investigaciones Científicas y Técnicas-Facultad de Ciencias Exactas, Físicas y Naturales (FCEF), Universidad Nacional de San Juan (UNSJ), San Juan, Argentina

⁴Departamento Geofísica y Astronomía, FCEF, UNSJ, Meglioli 1160 S (5407) Rivadavia, San Juan, Argentina

⁵School of Earth and Space Exploration, Arizona State University, P.O. Box 871404, Tempe, Arizona 85287, USA

Correspondence should be addressed to Ahmad Arnous; aarnous.aa@gmail.com

Received 20 August 2019; Revised 27 February 2020; Accepted 1 July 2020; Published 26 September 2020

Academic Editor: Sarah Roeske

Copyright © 2020 Ahmad Arnous et al. This is an open access article distributed under the Creative Commons Attribution License, which permits unrestricted use, distribution, and reproduction in any medium, provided the original work is properly cited.

Uplift in the broken Andean foreland of the Argentine Santa Bárbara System (SBS) is associated with the contractional reactivation of basement anisotropies, similar to those reported from the thick-skinned Cretaceous-Eocene Laramide province of North America. Fault scarps, deformed Quaternary deposits and landforms, disrupted drainage patterns, and medium-sized earthquakes within the SBS suggest that movement along these structures may be a recurring phenomenon, with yet to be defined repeat intervals and rupture lengths. In contrast to the Subandes thrust belt farther north, where eastward-migrating deformation has generated a well-defined thrust front, the SBS records spatiotemporally disparate deformation along structures that are only known to the first order. We present herein the results of geomorphic desktop analyses, structural field observations, and 2D electrical resistivity tomography and seismic-refraction tomography surveys and an interpretation of seismic reflection profiles across suspected fault scarps in the sedimentary basins adjacent to the Candelaria Range (CR) basement uplift, in the south-central part of the SBS. Our analysis in the CR piedmont areas reveals consistency between the results of near-surface electrical resistivity and seismic-refraction tomography surveys, the locations of prominent fault scarps, and structural geometries at greater depth imaged by seismic reflection data. We suggest that this deformation is driven by deep-seated blind thrusting beneath the CR and associated regional warping, while shortening involving Mesozoic and Cenozoic sedimentary strata in the adjacent basins was accommodated by layer-parallel folding and flexural-slip faults that cut through Quaternary landforms and deposits at the surface.

1. Introduction

Broken-foreland basins such as the foreland of the Cenozoic southern Central Andes evolve in areas where retroarc convergence is accommodated primarily along reactivated, high-angle structures (e.g., [1–3]). Rather than forming an extensive region of consistently sloping mean topography (e.g., [4]) and a well-defined deformation front (e.g., [5, 6]), as in orogenic wedges that host thin-skinned foreland fold-

and-thrust belts, uplift along high-angle structures in thick-skinned broken forelands is generally diachronous and spatially disparate (e.g., [3, 7]). These morphotectonic end members of foreland deformational styles are well exemplified by the Subandean foreland fold-and-thrust belt of Bolivia and north-western Argentina, and the broken foreland of the north-western Argentinean

Santa Bárbara and Sierras Pampeanas uplifts (Figure 1). The Santa Bárbara morphotectonic province is a seismically

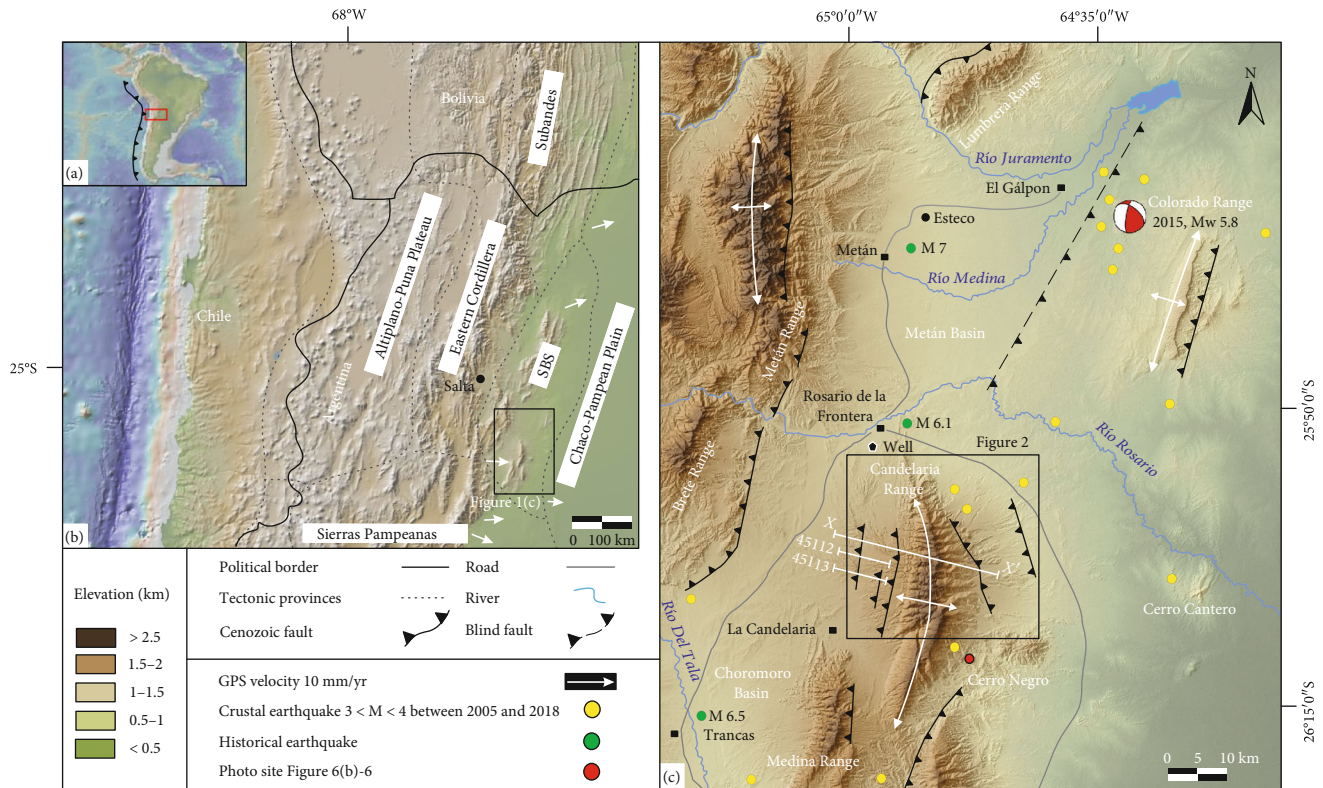


FIGURE 1: Regional morphotectonic setting of the northern broken foreland of the Argentinean Andes, with adjacent geological provinces. Inset (a) shows the location of the study area in the Andean context; the red box outlines the area covered by inset (b). (b) DEM of the north-western Argentinean Andes, with principal morphotectonic provinces [1] and GPS-velocity vectors [8]. Black rectangle outlines the area covered by inset (c). (c) DEM with 12.5 m spatial resolution of the Santa Bárbara System (SBS) of the broken foreland and its transition zones into the Eastern Cordillera (to the west) and the Subandean fold-and-thrust belt (to the north). Locations of damaging historical earthquakes (see text for references) and the GCMT focal mechanism of the 2015 Mw 5.8 El Galpón earthquake are also shown.

active low-strain region [8], characterized by discrete ranges of limited strike length that occur far away from the principal topographic front of the Andean orogen [4, 9] and that constitute a contractionally reactivated Cretaceous extensional province (e.g., [10–12]).

The recognition and definition of fault chronologies in low-strain broken forelands and within continental interiors located far from plate boundaries is an important and timely topic in tectonics [13, 14]. Such faults, often active over time scales of 10^3 to 10^4 years and with long recurrence intervals, present a major problem when seeking an overall understanding of the spatiotemporal characteristics of foreland deformation, as well as when evaluating seismic hazards [15–22]. Research topics that need to be investigated in order to better understand the ongoing tectonic and sedimentary processes that characterize such environments include the areal extent affected by tectonically active structures, the sub-surface geometries of faults, and deformational styles, as well as the impact of faulting on the geomorphic evolution. Addressing some of these topics may ultimately help to better establish the spatiotemporal characteristics of deformation and unravel the degree of activity of deformational processes in broken-foreland areas. The first and most basic step in such an endeavor is to determine fault geometries, and to assess fault kinematics and their possible relationships with

reactivated crustal anisotropies, prior to determining fault chronologies and deformation rates. We therefore chose such an approach in this study, focusing primarily on open questions relating to the seismotectonic character of the southeastern sector of the broken foreland of the Santa Bárbara System. In addition, we reviewed the impact of Quaternary tectonism on the landscape in this morphotectonic province.

We have examined suspected active faults in the piedmont zones of the Candelaria Range (CR), in the southern SBS at approximately 26°S (Figures 1 and 2), that may exist within the sedimentary cover rocks and whose activity may have been driven by blind thrusting in the basement rocks. Previous investigations have suggested that the main fault responsible for the uplift of the CR extends to the surface and that a fault in the western piedmont roots in the basement (e.g., [23–25]). However, these interpretations appear to be at odds with the structural relationships shown on the Geological Map of Salta [26]. This map indicates that the northern and southern terminations of the CR form an elongated basement uplift with doubly plunging drape folds, and it includes no indication of any major faults bounding the range. This suggests that the uplift of the CR could have been associated with motion along a blind thrust, while the adjacent piedmonts of the range may have been ruptured by structures possibly associated with flexural-slip folding in

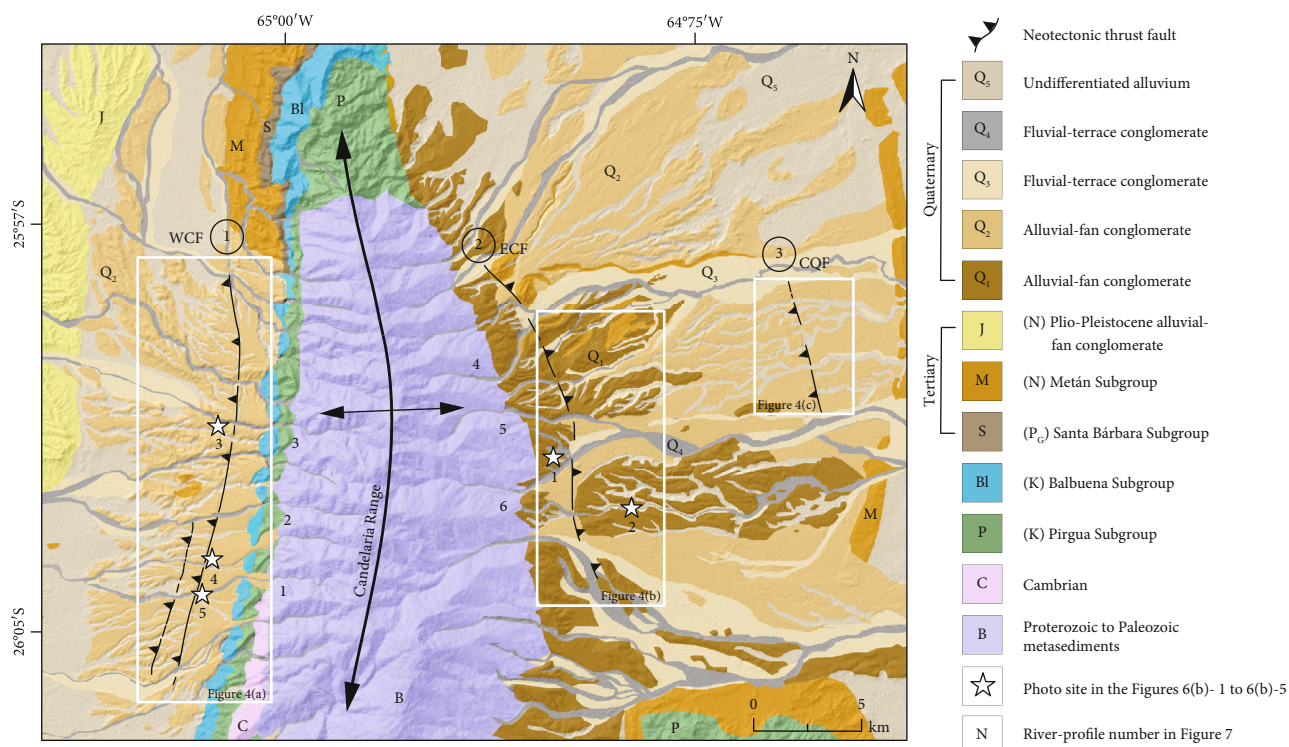


FIGURE 2: Geological map of the northern sector of the La Candelaria Range, based on a digital elevation model with a 5 m resolution (RESTEC, the Remote Sensing Technology Center of Japan). In addition to Paleogene, Neogene, Cretaceous, and basement rocks, we distinguish five stratigraphic levels of Quaternary piedmont deposits associated with alluvial fans and fluvial terraces. The locations of thrust faults of this study are shown. White rectangles indicate the locations of Figures 4(a), 4(b), and 4(c) in the vicinity of piedmont faults that were identified in this study: the West Candelaria fault, the East Candelaria fault, and the Copo Quile fault.

the sedimentary cover rocks and that resulted from ongoing shortening in the adjacent basement blocks.

Barcelona et al. [24] carried out a remote sensing and geomorphic analysis of the large-scale morphostructural characteristics of the greater CR region; they proposed a multistage tectonic evolution involving spatially separated thick-skinned and thin-skinned deformation styles. These authors identified a major fault scarp in the western piedmont of the CR and inferred a principal range-bounding fault delimiting the eastern flank of the CR. They furthermore suggested that a low mountain-front sinuosity along the western flank of the range is evidence of strong tectonic activity along a range-bounding fault.

For our research, we have built on these interesting results and carried out further investigations into the manifestations of Quaternary tectonic activity at three selected field sites. Valuable insights into the location and geometry of potentially active faults with poor morphologic expressions within humid regions can be achieved through a combination of geophysical and geomorphic analyses (e.g., [27–29]). In particular, the use of data combined from near-surface geophysical techniques, high-resolution digital elevation models (DEMs), and geomorphic field mapping has provided a robust methodology, which to reduce ambiguities in the deciphering of paleo-seismological features such as those suspected to exist within the SBS (op. cit.). We analyzed east- and west-dipping piedmont faults and tilted Quaternary alluvial-fan deposits on both flanks of

the CR that are suggestive of Quaternary tectonic activity. Fault scarps up to 30 m high appear to be the most pronounced features of tectonic origin in the intermontane basins of the SBS province. These scarps lend themselves to detailed inspection because they have been cut by rivers and expose deformed Tertiary sedimentary strata in the inferred hanging walls. In order to further assess the piedmont zones of the CR and to locate additional, possibly active faults and infer their geometries, we first conducted a geomorphic mapping. As a second step, we then used near-surface geophysical techniques, including 2D electrical resistivity tomography (ERT) and seismic-refraction tomography (SRT), across these fault scarps in order to characterize the fault geometry at depth. In a third step, we interpreted two oil-industry seismic reflection lines to link the observed surface structures to deep-seated geometries.

2. Geological and Geomorphological Setting

The seismically active foreland of the north-western Argentinian Andes between latitudes 23°S and 33°S is the type locality for broken forelands (Figure 1; [1, 30]); here, the accumulation of shortening during repeated earthquakes is suggested by variably deformed Quaternary deposits, tectonic landforms, and reverse-fault-bounded mountain ranges ([31][7, 24, 32–34]). In some cases, these mountain ranges are not bounded by faults with sufficient displacement to explain their relief, but they instead consist of extensive basement-cored antiforms

associated with sedimentary drape folds, underlain by blind faults (e.g., [2, 7, 32, 34, 35]). Taken together, these different structural and tectono-geomorphic phenomena reflect the complex long-term effects of protracted Cenozoic shortening in the broken Andean foreland, superimposed on crustal heterogeneities. As such, the structural character of this region is akin to the Cretaceous-Eocene basement uplifts of the North American Laramide province (e.g., [1, 3, 36, 37]) and the seismically active Tian Shan of Central Asia [38, 39].

The structures associated with the SBS record the inversion of the Cretaceous Salta Rift [10, 11, 23, 40]. At a latitude 23°S, this morphotectonic province transitions into the thin-skinned Subandes foreland fold-and-thrust belt (Figure 1). Ongoing spatially and temporally disparate tectonic activity within the SBS has created a topography with asymmetrically uplifted mountain ranges, intervening sedimentary basins, and tectonically forced drainage patterns and landforms with evidence of different stages of tectonic inversion [7, 24, 25, 32, 41–43].

The CR of the SBS belongs to a series of spatially separated, reverse-fault-bounded or basement-cored ranges associated with concealed faults within the broken foreland of the Andes (Figures 1 and 2; [24, 33, 44]). The uplift history of the SBS ranges is directly related to the spatially and temporally disparate eastward migration of Andean deformation within this sector of the foreland [12, 45–48]. This is in stark contrast to the tectonically active deformation front of the Subandes fold-and-thrust belt to the north, where the style of deformation is related to regional décollements that dip gently toward the west [49–56] (Figure 1).

The N-S trending basement-cored asymmetric antiform of the CR is located between latitudes 25.5° and 26.5°S, and between longitudes 65.5° and 64.5°W (Figure 1). The interior of the range exposes deformed Upper Precambrian to Lower Cambrian metasediments [57, 58], while folded sedimentary cover rocks are preserved around the flanks of the range and dip outwards [35, 59, 60]. These latter units comprise terrigenous and marine Cretaceous and Paleogene strata of the Salta Group, followed by continental clastic deposits of the Mio-Pliocene Orán Group [12] (Figure 3).

The oldest units of the Salta Group consist of red conglomerates and sandstones of the Pircua Subgroup [12, 61]. These syn-rift deposits are succeeded by post-rift sandstones and calcareous strata of the Balbuena Subgroup [62, 63], as well as lacustrine mudstones of the Santa Bárbara Subgroup [64]. These rift-related units are unconformably overlain by strata of the syn-orogenic Metán and Jujuy subgroups of the Orán Group. The majority of these strata are sandstones, conglomerates, and shaly deposits [26, 65].

These units are in turn unconformably overlain by Plio(?)–Pleistocene alluvial-fan conglomerates [26]. All piedmont zones of the CR are covered by these coarse deposits, which form an integral part of multiple, gently inclined geomorphic surfaces that occur at successively lower elevations away from the CR. Except for the lowest, active, alluvial-fan surface, all of these surfaces are isolated remnants of formerly contiguous and coalesced alluvial fans that have been incised since they were abandoned as active depositional environments.

3. Methods and Research Design

It is important to note that, while inspection of surface faults is relatively straightforward in the generally arid Sierras Pampeanas broken-foreland province (between latitudes 27°S and 33°S), as is also the assessment of seismogenic structures, particularly in the western part of that morphotectonic province (e.g., [66]), such features are more difficult to discern in the humid SBS province. A dense vegetation cover and rapid climate-driven modification of tectonically controlled geomorphic features render a seismotectonic evaluation of this region far more challenging (e.g., [7, 67–69]). In this environment, rupture zones, faults, and fold scarps have often been erosionally modified or even obliterated. Where vestiges of these tectonic landforms have been preserved, they are often concealed by dense vegetation [70] or have been further modified by anthropogenic influences. This compromises the collection of unambiguous geological, geomorphic, kinematic, and geochronological data used to characterize the level of tectonic activity.

Because of the dense vegetation cover within the CR piedmont zones that makes it difficult to detect fault scarps in the broken foreland, together with the highly dynamic surface-process regime that tends to rapidly modify seismogenic features in the landscape, we decided to use a combination of geological and geophysical methods to identify faults with possible Quaternary tectonic activity. Our field observations and a careful analysis of outcrops helped us develop and test a model of fault activity that could then be further evaluated using electrical resistivity images, seismic-refraction tomography, and seismic reflection profiles.

3.1. Tectono-Geomorphic Analysis of the CR Piedmonts. Our study of the geomorphic features was based on inspection of high-resolution digital elevation models (DEMs) and satellite imagery, with subsequent field validation for each fan on both sides of the CR. This allowed us to identify anomalies in the fluvial network and to unambiguously record different alluvial-fan generations within the piedmont zones. In order to develop a detailed geological map with particular emphasis on the youngest deposits and landforms, and to assist in mapping the different generations of alluvial fans and terraces, we used true color images from Landsat 8 (bands 2, 3, and 4) together with Google Earth images (Figure 2). Additional maps that included parameters such as relief, slope, and drainage characteristics were generated from two DEMs with spatial resolutions of 12.5 m and 5 m. These DEMs were generated from ALOS PALSAR data that we obtained from the Alaska satellite facilities [71]. The 5 m resolution DEM was acquired from RESTEC, the Remote Sensing Technology Center of Japan. We also analyzed the local relief and drainage characteristics using the TopoToolbox program [72, 73]. Finally, we used the 5 m resolution DEM to generate six longitudinal river and surface profiles to assist with our mapping and with interpretation of the tectono-geomorphic evolution of the piedmonts. The resulting river-gradient maps, together with the derived drainage networks and river/surface longitudinal profiles, helped us to identify the presence of fault and fold scarps.

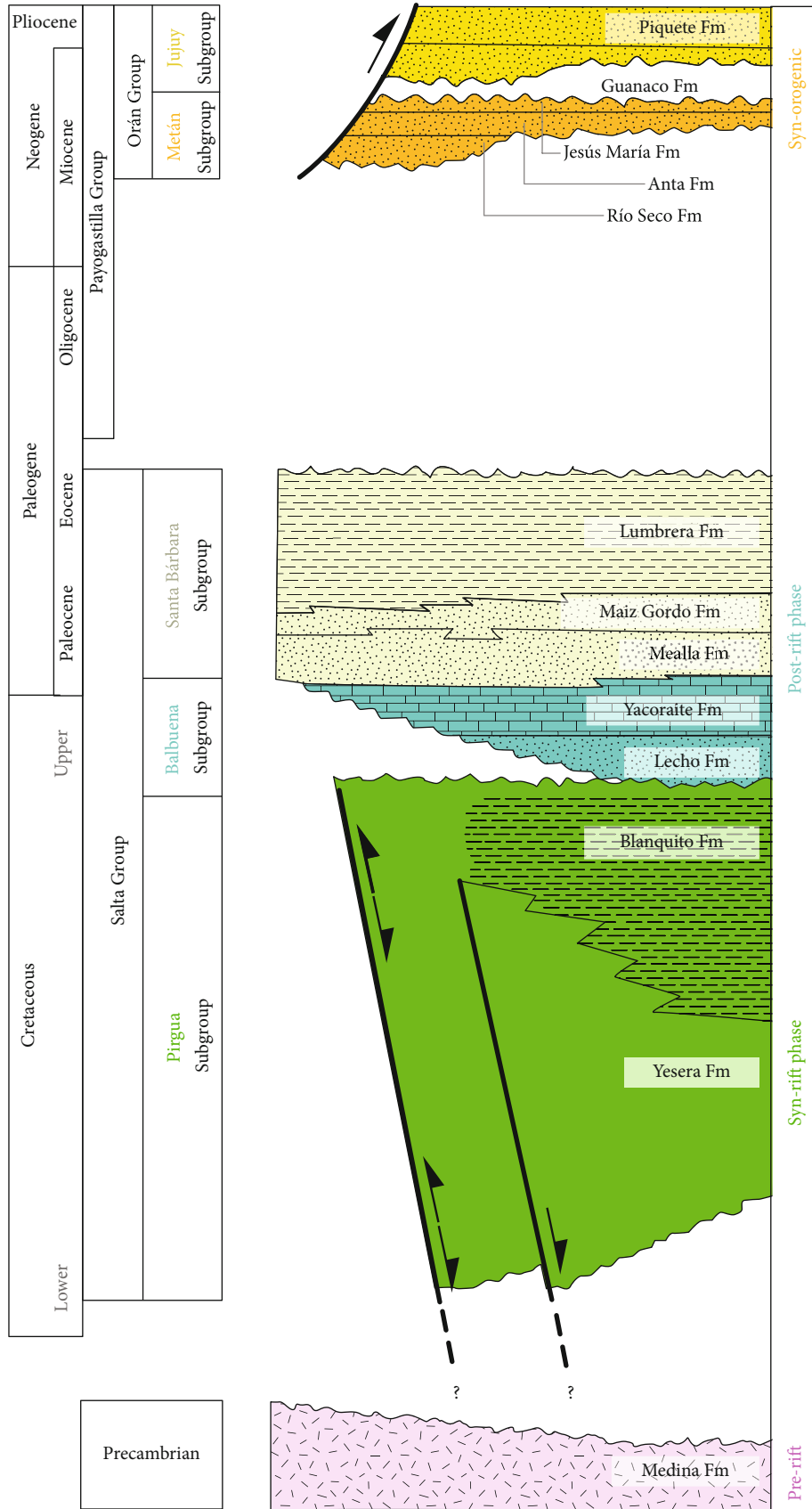


FIGURE 3: Stratigraphic column of the units exposed in the greater La Candelaria Range region, modified after Marquillas et al. [61], Carrera et al. [84], and Invernizzi et al. [103].

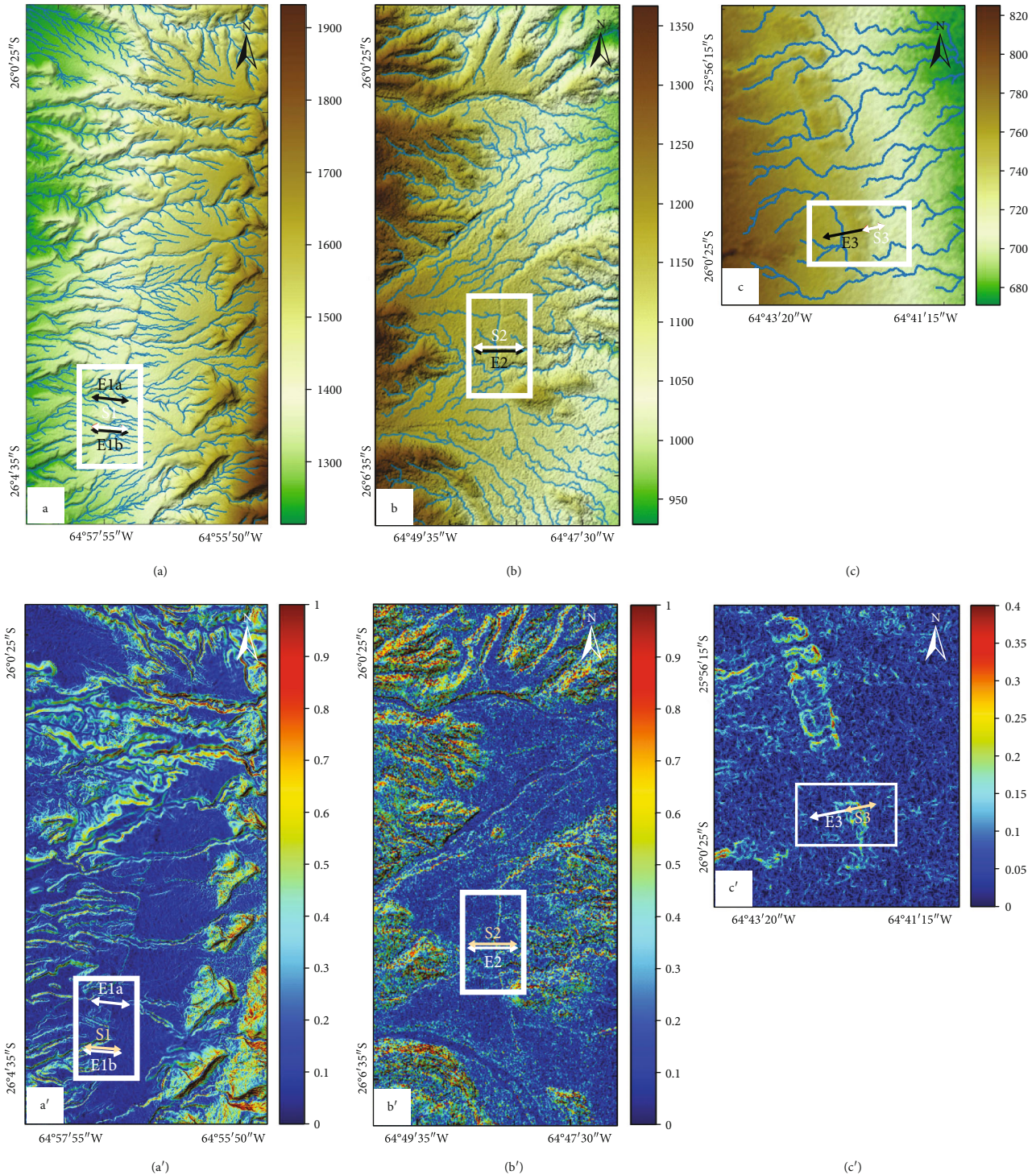


FIGURE 4: (a), (b), and (c) present digital elevation models (DEM) showing additional detail for fault scarps in the areas shown in Figure 2. The locations of electrical “E” and seismic “S” survey profiles crossing the fault scarps and the drainage network are also indicated, with diverted drainages shown in red. (a’), (b’), and (c’) correspond to the upper panels (a), (b), and (c) and show the slope, aspect, and north and east components of the gradient, in order to emphasize the fault scarps. (The gradient bar goes from 0 (blue color, which refers to the horizontal gradient) to 1 (red color, which refers to vertical gradient).)

3.2. Electrical Resistivity Tomography. A number of electrical resistivity tomographic (ERT) surveys were completed in the eastern and western CR piedmont areas to identify and characterize the geometry of fault zones at depth (Figure 4). The

depth of penetration in such surveys usually depends on the electrode separation and the length of the profile; for example, for an electrode separation of 6 m, the maximum depth of penetration ranges between 50 and 60 m. Resistivity

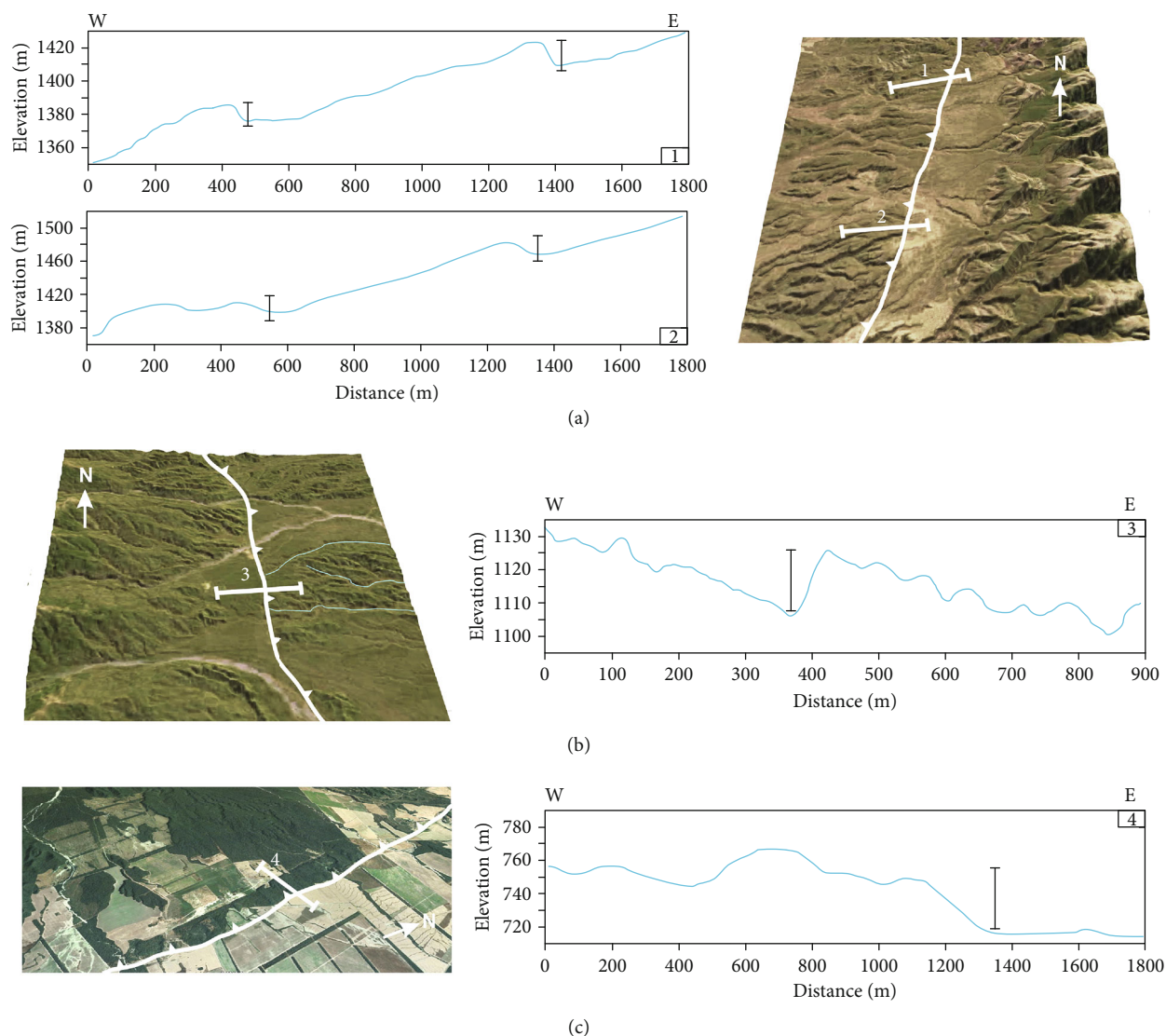


FIGURE 5: Annotated Google Earth images and elevation profiles of the three fault areas: (a) West Candelaria fault, (b) East Candelaria fault, and (c) the Copo Quile fault, farther to the east (see Figure 2). Note the fault scarps in each topographic profile.

contrasts between areas in the subsurface with different properties (e.g., [74]) and lateral heterogeneities can reveal fault architecture and the associated kinematics and deformation patterns, at least to some extent (e.g., [28]). The ERT surveys were all conducted with identical dipole-dipole electrode configurations and recorded with 48 electrodes at 6 m spacings, to achieve 288-m-long profiles at each of the selected survey sites. The profiles were designed with orientations perpendicular to the scarps of the suspected faults, with each profile centered on the highest point of the scarp to ensure that any possible fault continuation on either side of the surface expression of the structure was also covered. We chose to conduct our surveys during the arid season, when the water table level typically drops to between 50 and 60 meters below the surface; this information was obtained from farmers whose water supplies depend on local wells, which are regularly monitored. In order to achieve greater penetration along the East Candelaria piedmont profile, we followed an ephem-

eral stream channel across the scarp of the inferred fault (Figures 4(b) and 5). We used an ARES georesistivity meter from GF Instruments Inc. (<http://www.gfinstruments.cz>) to obtain fully automated measurements.

The apparent resistivity values were automatically inverted using RES2DINV software [74], which follows a 2D inversion method developed by Loke and Barker [75]. This routine is based on a smoothness-constrained least-squares inversion implemented using a quasi-Newton optimization technique [76].

The optimization adjusts the 2D resistivity model by iteratively minimizing the residuals of the apparent resistivities. The root mean-square (RMS) error is then taken into account when evaluating the efficiency of the minimization process in the least-square approach, for all data sets and configurations. We considered an RMS error < 10 good enough for the model to be accepted. For the two profiles on the western flank of the CR (Profiles E1a

and E1b; Figures 2, 4(a), and 5), the inversion yielded good results after four iterations using the electrical data obtained for Profile E1a. The eastern Profile E2 (see location in Figures 2, 4(b), and 5) also yielded an acceptable inversion model after four iterations. Finally, for the easternmost profile (E3) on the eastern flank of the CR region (see location in Figures 4(c), and 5), we obtained a feasible model after just two iterations.

3.3. Seismic-Refraction Tomography. Following our geomorphological and morphometric analyses and the ERT surveys, we carried out three seismic-refraction tomography surveys (S1, S2, and S3) at approximately the same locations as the ERT surveys (Figures 2, 4, and 5). We used a GEODE Exploration Seismograph connected to 24 vertical-component 4.5 Hz geophones spaced 10 m apart (Figure DR1). The seismic source consisted of an accelerated weight of 100 kg and a 2 m height-acceleration path; we used three impacts (or shots) per site on average, in order to be able to improve the signal-to-noise ratio by stacking the three sets of results for each shot point. On seismic line S1, we also used two additional shot points, at 30 m and 70 m offsets from the first geophone along the profile line. This configuration was repeated symmetrically for the last geophone in the seismic line, as shown in Figure DR1 in our data repository. Other additional shots were used at 125 m, 185 m, and 255 m from the first shot position (Figures 2–4 and DR1). For seismic line S2 (Figures 2 and 4 y DR1), we carried out shots at 5, 30, and 70 m offsets from the first geophone on the line, and at 5, 30, 70, and 110 m offsets from the last geophone. Three additional shots were also made at intermediate positions, at distances of 125, 185, and 255 m from the first shot. For seismic line S3 (Figures 2 and 4), we carried out seismic acquisitions using shots at 5 m and 35 m offsets from the first geophone and shots at 5 m and 35 m offsets from the last geophone. Four additional shots were also used at intermediate positions 90, 145, 170, and 210 m from the first geophone. The S1 seismic line was therefore the longest and the S3 seismic line the shortest in our study, due mainly to access limitations.

We processed the seismic-refraction tomography data using SeisImager/2DTM software (available from <http://www.geometrics.com>), which follows a methodology proposed by Hayashi and Takahashi [77]. This method uses a direct modeling algorithm developed by Moser [78] and Hayashi and Takahashi [77], based on a technique sensitive to inhomogeneities in the subsurface represented by lateral changes in seismic wave velocities. We performed an inversion for hand-picked first *P*-wave arrivals. By comparing observed travel times with theoretical travel times from a preliminary layered model, we generated a final seismic velocity model following ten inversions for each seismic profile. Our results were consistent, with an RMS error of 3.2% for the western CR line (S1), an RMS error of 4.1% for seismic line S2, and an RMS error of 3.6% for seismic line S3. The residuals were determined quantitatively after each iteration and cross-checked qualitatively for the space distribution of mod-

eled ray paths. Using different initial seismic velocity models and good ray-path coverage with the inversion of the 2D *P*-wave velocity refraction data, the results were shown to be consistent to a depth of about 80 or 90 m (e.g., [79]).

3.4. Seismic-Reflection Stacks and Well-Log Data. We obtained well-log data from one petroleum exploratory well and six oil-industry seismic reflection profiles provided by Yacimientos Petrolíferos Fiscales (YPF) of Argentina. We used the eastern half of lines 45112 and 45113 (Figure 1), which were located in the northern part of the intermontane Choromoro basin on the western side of the CR. Both lines were approximately perpendicular to the CR main axis (Figure 1). The Rosario de la Frontera Norte x-1 well was located to the south of Rosario de la Frontera town, northwest of the CR (Figure 1). Importantly, the seismic lines cross the homocline that developed in the sedimentary cover units on the western flank of the CR as a result of uplift of the range. In this area, the partially eroded sedimentary cover forms a rather straight line of westward-sloping flatirons at the contact with the piedmont gravels. The approximately east-west oriented seismic reflection lines cover a length of about 25 km, with a separation of about 4 km.

The SEG-Y seismic-line data were analyzed together with the well logs and combined with the surface geology to derive a subsurface geological model. We then compared this model with the shallow-penetration geophysical data that we had obtained. We first applied a frequency filter to remove residual noise and then performed a time-to-depth conversion using Move2D software (Petroleum Experts, Midland Valley Exploration Ltd.), making use of seismic velocities from the well data and the YPF seismic data. We next used the uppermost units of the sedimentary strata in the well log to tie stratigraphic boundaries to the seismic stacks for the interpretation. The well depth was 3200 m, which means that it penetrated the stratigraphy (Figure 3) from the Quaternary (Piquete Formation) to the Tertiary, terminating in the Upper Cretaceous (Lecho Formation, Balbuena Subgroup). We also extrapolated imaged strata from surface outcrops on the western flank of the CR, where the underlying sedimentary strata (including Lower Cretaceous units) are exposed.

These data were combined together and integrated into a structural model based on an earlier analogue model from Seggiaro et al. [80]. The cross-sections were forward-modelled using 2D area-balancing techniques, with the algorithms provided in the Move2D program, in order to obtain the best geometric match between the observed geological field conditions and the model. Trishear techniques (e.g., [81]) were used to derive the geometry of the basement fault responsible for the drape folding of the sedimentary cover rocks.

4. Results

The broken Andean foreland has been strongly influenced by tectonic processes that have impacted the Quaternary landscape evolution, to the present day. This influence is manifested by drainage reorganization (Figures 4(a)–4(c)), the tilting of the various alluvial-fan surfaces, and the presence

of fault scarps. In this section, we first report on the results of our geological and geomorphic observations in the CR. We then characterize faults in the CR piedmonts using the results from ERT and SRT surveys. Finally, we use seismic reflection profiles to extend our near-surface interpretation of possible fault geometries down to greater depths. In this study, we have identified five fault scarps in the CR piedmonts through remote sensing, but due to limited accessibility we had to restrict our data collection in the field to three of these structures, which we named according to their locations: the West Candelaria fault in the western CR piedmont, and the East Candelaria and Copo Quile faults in the eastern CR piedmont (Figure 2). Over time, erosional modification has smoothed the profiles of these scarps to the extent that they may now appear at first sight to be fold scarps. However, the straightness of the scarps and the narrow widths of the features, together with the data from our geophysical analyses (see below), indicate that the fault tips must be within at most a few meters of the surface, but most likely they broke the surface.

4.1. Tectono-Geomorphic Analysis. We were able to use the elevation of the fan surfaces in the CR piedmont, their lateral continuity and degree of dissection to separate them and associated fluvial terraces into five different geomorphic and stratigraphic units. These units record stages of fan formation, subsequent incision, and renewed fan deposition at subsequently lower elevations within the piedmont. In the westernmost sector of our study area, there are dissected and deformed conglomerates (Figure 2) that probably have a similar alluvial-fan origin as closely spaced conglomeratic alluvial-fan remnants. Episodic incision has generated four stratigraphic units that correspond to different levels of alluvial fans and fluvial terraces (Q_1 - Q_4) that define a staircase morphology. The youngest unit (Q_5) is an undifferentiated conglomeratic Quaternary sediment fill in the present-day drainage channels (Figure 2). The first, and topographically highest fan surfaces and their deposits (Q_1) are only found on the eastern side of the CR (Figure 6(a)-1); these are the fan surfaces closest to the range and they have been deeply incised, with locally high relief of approximately 50 m (Figures 6(b)-1 and 6(b)-2). They comprise boulder conglomerates and coarse, matrix-supported conglomerates, often intercalated with thin layers of sand and silty clay (Figures 6(b)-1 and 6(b)-2). These older fan surfaces appear to have been tilted by tectonic warping following their formation because their inclination is locally greater than 5° and, in some cases, up to 12° . If the gradients of the fan remnants are extrapolated back toward their source areas in the CR, the proximal fan surfaces would project to the highest levels of the mountain range and they would not reach the mountain fronts, where the streams would have originally deposited the conglomeratic fan gravels. This suggests that the incision of the oldest fan surfaces was closely linked to tectonism in the piedmont zones, which may also have been accompanied by a drop in base level. Such a tectonic interpretation is supported by the polymict composition of the fan gravels, which includes rock types that are exposed along the entire range and is not restricted to the basement rocks of the high range

interior (Figure 6). A monomict, basement-dominated composition would be expected had the piedmont fans and terraces been originally associated with such a high source area.

The second, less dissected group of fan deposits and corresponding surfaces (Q_2) is found on both sides of the CR (Figure 6(a))-2). These fans occupy a lower part of the piedmont and are characterized by lower local relief. The exposed fan strata consist of coarse conglomerates with overlying layers of silt and interbedded gravels (Figures 6(b)-3 and 6(b)-4).

The Q_2 fan remnants of the west CR piedmont are characterized by well-lithified conglomerates that dip up to 9° toward the west (Figure 6(b)-5). These units directly overlie Cretaceous and Paleogene sandstones and siltstones that dip at between 25° and 30° toward the west.

Fluvial terraces are sculpted into the older alluvial-fan deposits. The terrace (Q_3) comprises coarse to very coarse basement gravels from the interior of the range, together with intercalated sandy to silty layers. The exposed cover gravels of the younger fluvial terrace (Q_4) are matrix-supported and conglomeratic. The youngest unit (Q_5) defines aggrading strata within the main piedmont drainages and their tributaries (Figure 2).

4.1.1. Eastern Piedmont. The oldest eastern fans (Q_1) have been offset by the East Candelaria fault (Figures 2, 5, and 6(a)-1, 6(b)-1, 6(b)-2) with an east-side-up displacement. These fans are the most eroded and are now only represented by scattered surface remnants along the length of the eastern piedmont of the CR. Activity along the East Candelaria fault interrupted the eastward-directed drainages from the CR and started the dissection of the fan surfaces; the younger Q_2 alluvial-fan surface was then generated at a lower elevation (Figures 2 and 4). The East Candelaria fault is located 2 km to the east of the range (Figures 2, 5 (Profile 3), Figures 4(b) and 4(b')). It strikes approximately north-northwest, extends for about 20 km, and cuts through the geomorphic surfaces associated with both the Q_1 and Q_2 alluvial-fan deposits. The vertical offsets of the fan surfaces are about 20 m (Figure 5, Profile 3). In the south-eastern portion of the CR piedmont, the surface that corresponds to Q_1 is displaced by 20 m relative to the elevation of the Q_2 surface, while in the northern part of the fault the offset is at least 30 m (Figures 4(b) and 4(b')). The light blue color in Figure 4(b') that represents the smooth surface of Q_2 (Figure 4(b)) also highlights the spatial arrangement of the drainage and the relationships between the abandoned Q_1 fan surface and the younger Q_2 fan surface. The older Q_1 fan surface was probably incised and eroded after movement along the East Candelaria fault had uplifted the fan surface, forcing the drainage to flow northward.

To the east of the East Candelaria fault is the Copo Quile fault scarp. This is the shortest of the faults in the eastern piedmont of the CR that appear to be associated with Quaternary activity, extending for about 8 km along a north-northwest strike direction (Figure 5, Profile 4). This fault cuts the Q_2 alluvial-fan gravels and offsets them vertically by about 25 to 30 m (Figure 4(c)). From Figure 4(c'), it can be

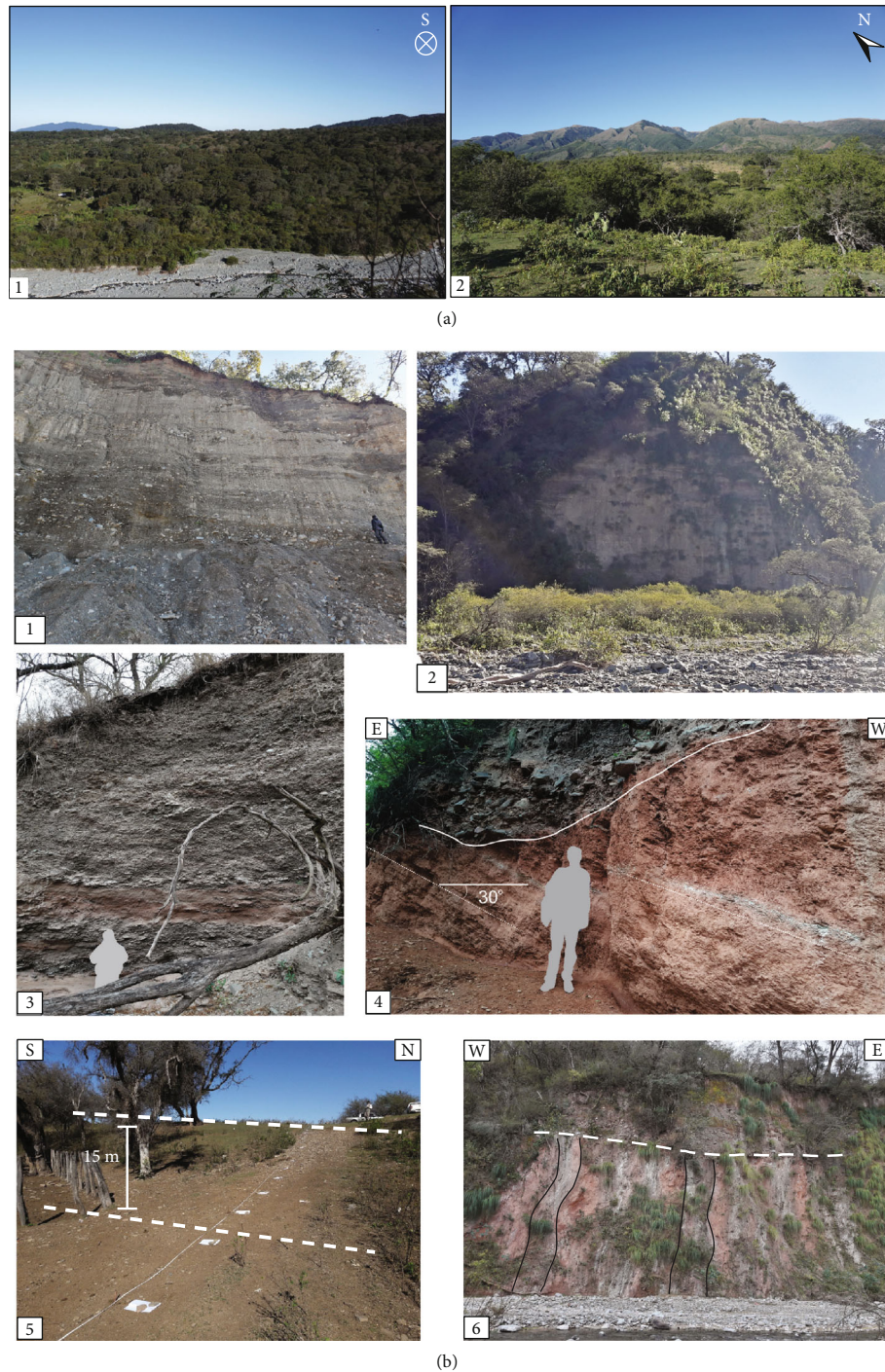


FIGURE 6: (a)-1 shows the southward view of the Eastern Candelaria Range piedmont. In the foreground, metamorphic gravelly deposits of an eastward-flowing stream sourced in the basement of the Candelaria Range interior. In the middle sector of the photo, the eastward-tilted erosional remnants of the Q_1 alluvial-fan surfaces are visible (photo taken from a Q_1 remnant fan). (a)-2 shows the north-eastern view of the central sector of the western Candelaria Range piedmont. The contact between the vegetation-covered alluvial fans and the range is straight due to the intersection of the gravel-covered piedmont and the westward-dipping triangular flatirons of the Cretaceous-Paleogene sedimentary rocks and the difference in erodibility between the rocks exposed at the range front and the piedmont strata. Photo taken from the hanging wall of the West Candelaria fault; the break in slope in the foreground corresponds to the degraded fault scarp. (b) Field views of faulted Quaternary gravel deposits from four alluvial-fan locations on both flanks of the Candelaria Range. The numbers in the corner of each image indicate the locations in Figure 2. (b)-1 and (b)-2 show the Q_1 alluvial fan on the eastern flank of CR. (b)-3 and (b)-4 show the Q_2 alluvial fan on the western flank of the CR. (b)-4 illustrates the unconformity between Q_2 and the underlying Cretaceous sediments. (b)-5 shows the scarp of the West Candelaria fault. (b)-6 shows Santa Bárbara strata in the south-eastern part of the CR, dipping steeply toward the east.

seen that the slope of the fan surface offset by the fault is gently inclined toward the east. This setting clearly documents that the fluvial network in this area has been diverted by faulting. Some of the drainages were able to maintain their eastward flows while the Copo Quile fault was active, but others were forced to change their courses southward to avoid the growing topography associated with the active fault.

4.1.2. Western Piedmont. In the western part of our study area, the conglomerates of the remnants of the oldest Plio-Pleistocene piedmont strata (Unit J) are incised by streams sourced in the CR (Figures 2 and 4). These gravels are in angular unconformable contact with the Plio-Pleistocene strata of the Jujuy Subgroup [7, 26]. The Q_2 fans in the western piedmont were also affected by faulting. The West Candelaria fault, with its prominent, 17-km-long, uphill-facing scarp strikes parallel to the orientation of the CR (Figures 2 and 4). It is a layer-parallel structure between the Neogene strata of the Metán Subgroup that dips at 30° toward the west. The fault offsets the Q_2 alluvial fan vertically by up to 20 m (Figure 5(a)). The fault trace is clearly visible as a straight line on satellite imagery, in the DEM, and in the field (Figure 4(a)), even though the scarp is rather gentle and has been erosionally modified. A second fault trace is evident to the west of the central part of the West Candelaria fault (Figures 5 and 6(b)-5 (Profiles 1 and 2)). Outcrops exposed in rivers cutting across these structures reveal an angular relationship between the tilted Quaternary conglomerates and the underlying deformed Tertiary strata (Figure 6(b)-4), confirming the sustained deformation in the piedmont. The smooth Q_2 fan surface terminates abruptly against the straight fault-line, but the fan level continues across it in the form of a tilted, dissected fluvial terrace. These relationships are well expressed on our slope map of the western flank of the CR (Figure 4(a')), where the smooth Q_2 surface (blue) abuts the flatiron landforms of the Mesozoic rocks (red and yellow-colored sectors) that cover the westernmost flanks of the CR. Beyond the fault scarp to the west, the slope remains gentle, but this area is incised by numerous ephemeral streams.

As in the eastern piedmont, our field mapping and visual correlation in the field is based on the geological map of Metán [26], lateral pinch-outs and the chronology developed for the SBS basins by Hain et al. [7], and we conclude that all incised and erosionally modified surfaces in the western piedmont belong to the Q_2 fan surface.

To analyze the tectonic imprint on the landscape in greater detail, we generated six longitudinal river and geomorphic-surface profiles across the western and eastern slopes of the CR, using our 5 m resolution DEM data (Figure 7). The longitudinal profiles of the present-day river courses across the western flank of the CR do not show any knickpoints at the fault locations or within the basement areas. We therefore suggest that faulting in the piedmont zones along the West Candelaria fault was followed by protracted incision and the reestablishment of a concave longitudinal river profile. It is not known when the reestablishment of this equilibrium profile was completed, but the gentle gra-

dient suggests that either the West Candelaria fault did not remain to be active for long, or the tectonic forcing was relatively weak compared to the erosional processes. Knickpoints do exist within the CR (Figure 7, Profile 5), but rather than indicating tectonic forcing they are interpreted to be related to outcrops of resistant Precambrian basement rocks.

The topographic profiles across the inclined alluvial-fan surfaces clearly reveal the sites of faulting responsible for the two uphill-facing scarps of the West Candelaria fault and the less well-expressed fault to its west (Figures 2, 5 (Profiles 1 and 2), Figures 4(a) and 4(a')). In the longitudinal profile, the fan sectors to the west of these faults are more steeply inclined than would be expected for an equilibrated alluvial-fan profile.

In light of the regional compressional tectonics affecting the Santa Bárbara System, these observations suggest that the greater inclination of the fans (between 5° and 12°) to the west of the West Candelaria fault reflect tilting in the hanging wall of possibly west-dipping, thrust faults that have generated east-facing scarps (see Sections 4.2, Section 4.3, and Section 4.4 describing the results of our geophysical surveys).

Finally, our geomorphic analysis and the extensive field inspections of all major drainages that originate in the CR and cross the transition area between the range and the piedmont zones have revealed that a previously reported major range-bounding fault on the eastern side of the CR (i.e., [24, 35]) does not in fact exist. None of the alluvial-fan surfaces covering the transition area between the range and the piedmont are offset by faulting, nor do any of the river-cut exposures reveal any evidence of deformed or cataclized rocks within a fault zone. Knickpoints do exist in the metamorphic basement rocks of the range interior and are most likely controlled by lithology or they reflect regressive knickpoints related to upstream-migrating incision processes related to regional-scale basement upwarping. Importantly, no knickpoints exist in the longitudinal profiles crossing the range front, however. Taken together, the east-west asymmetry of the range and its doubly plunging northern and southern terminations must therefore be the result of differential tilting, which we suggest is likely to have been related to blind faulting beneath the range. In contrast, the three main scarps in the piedmont zones associated with the West Candelaria, the East Candelaria, and the Copo Quile faults are interpreted as being of related to surface rupture (Figure 4). These inferred fault scarps are further analyzed below using our newly acquired geophysical data.

4.2. ERT and SRT Results for Profiles E1a, E1b, and S1 (West Candelaria Fault). The E1a and E1b ERT profiles across the western CR piedmont (Figures 2 and 4) were measured perpendicular to the fault scarp, as shown in the geological and slope maps (Figures 2 and 4(a)). From the limited amount of outcrop in the area that is accessible for direct inspection, together with the well-log information, we inferred that all sedimentary rocks in the immediate subsurface are of Cretaceous or Tertiary age, and that these are covered by Quaternary alluvial-fan gravels (Figure 6(b)-4). Our geological observations in the river exposures across the scarp indicated

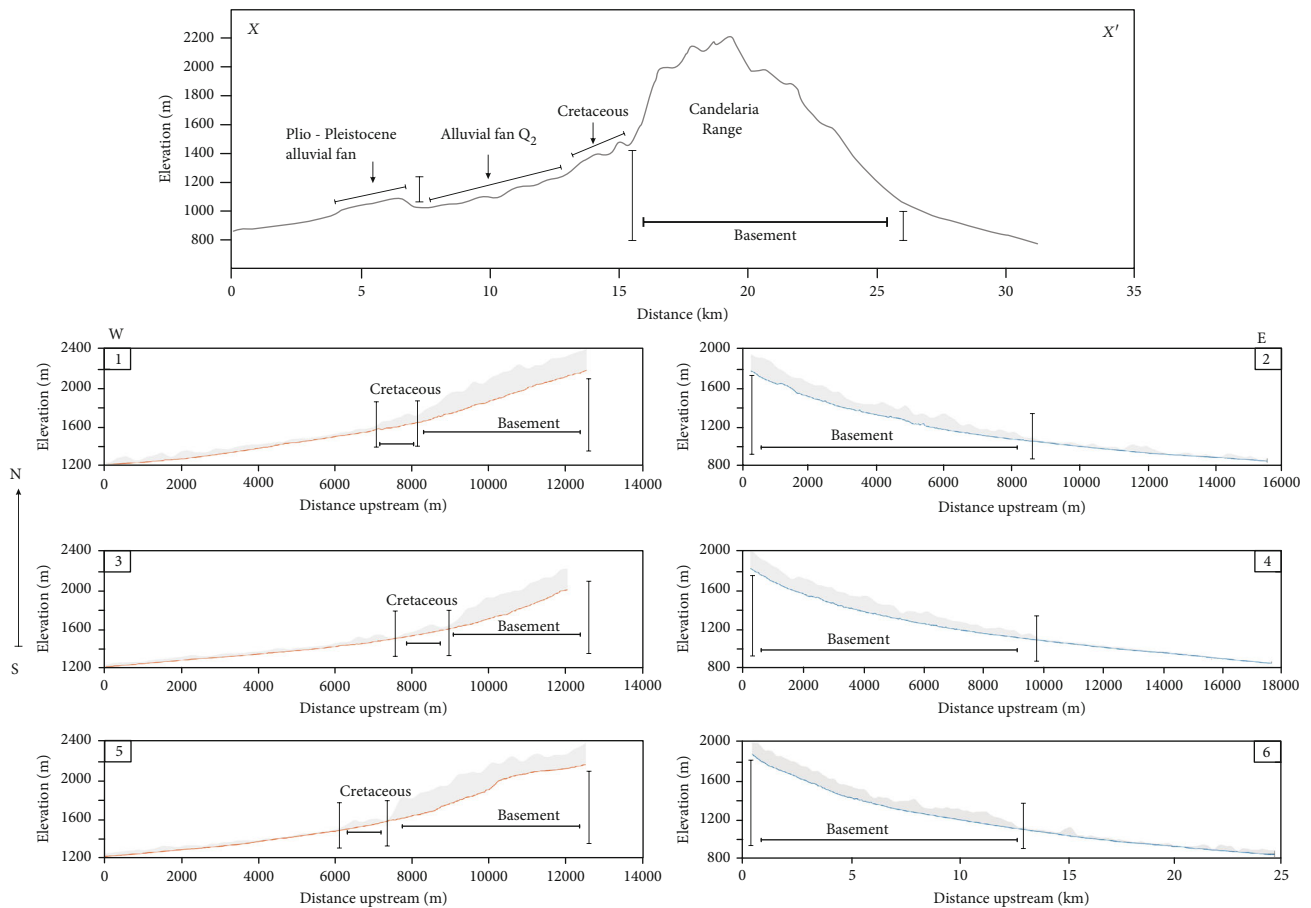


FIGURE 7: Topographic profile XX' (see Figure 1 for location) with threefold vertical exaggeration. We used the same profile in Figure 12. Profiles 1-6 depict longitudinal river profiles (see Figure 2 for river locations); gray areas represent topography in a 2 km wide swath along the river course.

that faulting was layer-parallel and related to flexural slip; this faulting did not rupture the Metán Subgroup strata obliquely. In addition, we observed the alluvial-fan sediments in an angular unconformity with the Metán Subgroup strata and the associated alluvial-fan remnants are tilted westward. We carried out tomography surveys at two sites where the faulted nature of the scarp could be inferred from the vertical offsets (Profile E1a shows a 3 m offset; Profile E1b shows a 15 m offset). The resistivity values obtained ranged between 6 and 800 ohm*m, with an RMS error of 5.1 after four iterations. The maximum penetration depth was about 65 m. A significant lateral variation in resistivity from west to east was found between -20 and 20 m of profile length, indicating an abrupt horizontal change from low to high-resistivity zones at elevations of between 1360 and 1350 m. In the eastern part of the same survey, at elevations of between 1370 and 1360 m, and between 0 and 100 m of profile length, we recorded a low-resistivity layer that thinned towards the east. Immediately below this low-resistivity layer, we imaged a highly resistive layer of approximately double the thickness of the layer above it. In the western part of the profile, we noted an upper high-resistivity layer about 5 to 10 m thick, overlying a low-resistivity layer.

Approximately 1100 m further to the north, we measured electrical properties along Profile E1a using the same survey configuration (length: 288 m; number of electrodes: 48; electrode spacing: 6 m; quadripoles: 802; Figure 8). After four iterations, we obtained a reliable RMS error of 3.0%, with resistivity values varying between 7 and 1100 ohm*m and a maximum penetration depth of 65 m. This profile showed high resistivities in the upper 25 m along its entire length, with maximum values of 909 ohm*m. The section between -60 and 10 m of profile length (Figure 8) emerged as a conductive zone, where the resistivity values decreased to 7 ohm*m at depths greater than 23 m. This is similar to observations along the southern profile (E1b), although in that case a topographic step exists at the surface and the amplitude of the resistivity anomaly is smaller. We observed on Profile E1b an abrupt vertical reduction in resistivity with increasing depth immediately above the conductive zone described above. Both profiles on the western flank of the CR showed a coherent subsurface resistivity structure.

The S1 seismic tomography profile (Figure 8), which was recorded at the same location as the ERT Profile E1b (Figure 4), revealed a seismic velocity structure consistent with V_p values that increased with depth. We noted lateral

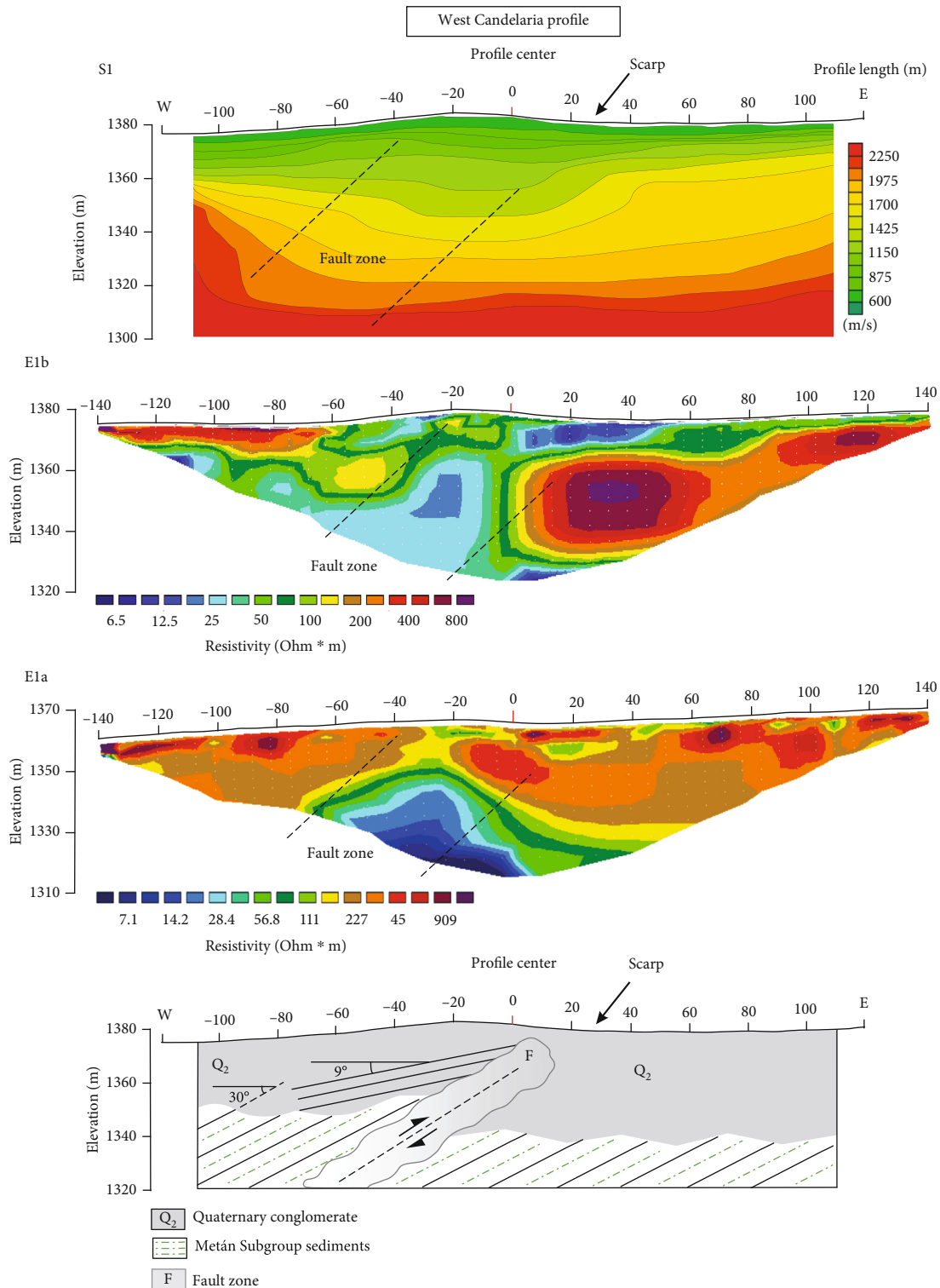


FIGURE 8: Seismic-refraction tomography results for Profile S1 across the West Candelaria fault (see Figure 4(a')) for location), with P -wave velocity contours every 275 m/s. Electrical resistivity tomography along Profiles E1a and E1b (see Figure 4(a')) for location). The selected inverse model was obtained after four iterations with an RMS error percentage of 5.1 for E1a and 3.0 for E1b. A dipole-dipole array was used with an electrode spacing of 6 m. Maximum penetration depth was approximately 60 m. Electrical resistivity tomography along Profile E1a, is located 1 km to the north of Profile E1b (see Figure 4(a')) across the West Candelaria fault. Note the good correlation between the inferred position of the fault, the displacement of the high-velocity layers for S1, and the location of the fault as inferred from electrical resistivity results for Profiles E1a and E1b (Figure 4). Schematic cross-section showing field observations combined with the interpretation of Profiles E1a and E1b, pointing out the fault location and kinematics.

variations in V_p close to the inferred fault, suggesting localized variations in thickness. The different velocity layers were continuous along the entire E-W profile. The layer characterized by a V_p of approximately 1270 m/s recorded an increased thickness in the central part of the profile; this is in good agreement with the topography of the ground surface above. Another anomaly in seismic velocities was found between about 1360 and 1340 m elevation and at a distance of between 20 and 70 m along the profile. An approximately 10-m-thick low-velocity layer was recorded at a shallow depth in the central part of the profile between -30 and 10 m of profile length.

4.3. ERT and SRT Results for Profiles E2 and S2 (East Candelaria Fault). The E-W orientation of the E2 and S2 profiles is perpendicular to the inferred orientation of the East Candelaria fault at depth (Figures 2 and 4). This structure has a minimum topographic offset in excess of 22 m. We used a similar electrode configuration to that used for Profiles E1a and E1b on the west side of the CR. After four iterations, the inversion resulted in a reasonable RMS error of 4.2%. The resistivity model displayed an almost vertical major discontinuity close to the center of the profile, coinciding with the position of the north-northwest oriented morphological scarp. The western half of the profile is dominated by high-resistivity values, while lower values (between 1 and 10 $\text{ohm}\cdot\text{m}$) are characteristic of the area to the east of the scarp. The thin uppermost layer exhibits high resistivities across the entire E-W transect.

Results from the S2 seismic profile were obtained from the same location as the E2 electric profile; this profile shares the same central reference point (Figure 9). The identified velocity layers are continuous from west to east. The shallower layers are parallel to the surface and therefore have a gentle eastward inclination. Between -20 m and 80 m horizontal distance along the profile, layers with high velocities get closer to the surface. These high-velocity layers define an area in the central part of the profile in which the thicknesses of the different layers decrease noticeably as they approach the surface; the sediment cover in this central part of the seismic line was negligible. We note that the vertical shift in velocities for layers in the eastern portion of the velocity model was consistent with the location of the resistivity discontinuity in the corresponding model.

4.4. Results for ERT and SRT Profiles E3 and S3 (Copo Quile Faults). East of the East Candelaria fault and at a distance of approximately 10 km from the eastern flank of the CR, the E3 profile (obtained by merging three intersecting electrical profiles) crosses a wedge-like structure with a total length of 576 m (Figures 2 and 4); we used a total of 1869 quadrupoles (Figure 4(c)) to measure this section.

The resistivity results indicate a range between 0.5 and 250 $\text{ohm}\cdot\text{m}$. The final model of this profile was obtained after two iterations, with an RMS error of 7.3%. Along this profile, we identified a high-resistivity layer in the upper 15 m, with a gentle westward inclination; at a 480 m horizontal distance of profile length, the inclination of this layer changes to an easterly orientation.

At 288 m of profile length (central part of the profile) in the shallow part of the profile, there is a westward-inclined layer (orange color) toward the 0 m mark of the profile; this layer becomes progressively deeper and more conductive. The layer also becomes thicker to the west and is covered by a thin layer with lower resistivities (1 to 17 $\text{ohm}\cdot\text{m}$). On the eastern shallow part of the traverse from 288 m of profile length until the eastern end of the profile, there is a high-resistivity layer with a thickness of approximately 5 m. Immediately below the high-resistivity surface layer (Figure 10; red color), there is a layer about 30 m thick (blue and green colors) of low resistivity that is inclined westward; this layer changes its inclination to an easterly inclination at about 480 m horizontal distance in the eastern (elevation of 690 m) sector of the profile. Between 384 and 480 m horizontal distance of profile length and at elevations between 660 and 650 m, there is a high-resistivity area in the east that is characterized by resistivities of about 40 $\text{ohm}\cdot\text{m}$ (yellow area below the blue layer in Figure 10). This high-resistivity layer appears to have broken through the conductive layer above it (blue layer).

Our results from the S3 seismic profile covered the easternmost 250 m of the E3 electrical profile (Figure 10). The modeled velocity profile indicates high velocities (>2500 m/s) close to the surface in the westernmost part of the profile, at an elevation of 672 m, with a strong vertical velocity gradient; the isovelocity layers were inclined at approximately 30° toward the east, before becoming subhorizontal in the eastern part of the profile, at an elevation of 652 m. The low-velocity layers became distinctly thinner towards the west, while layers with velocities between 1175 and 2000 m/s are thicker. Results from the eastern end of the profile thus indicate a horizontally layered seismic velocity structure. Layers with intermediate velocities reach the surface between 60 and 80 m horizontal distance along the profile indicating a lack of horizontal continuity in the seismic velocity layers.

4.5. Interpretation of Seismic Reflection Data. The two stacked seismic reflection profiles are located a few kilometers to the west of the West Candelaria fault. We also used well-log data from a petroleum-exploration borehole located near the town of Rosario de la Frontera (Figure 1) to tie the identified reflectors to geological units observed in the field. We were thus able to identify the entire stratigraphic column on the basis of vertical variations in acoustic impedance associated with the different layers. The low-intensity reflections with a chaotic signal and poor lateral continuity are likely due to the imaging of metamorphic basement rocks at a depth of 4100 m. An angular unconformity was imaged between basement rocks and the overlying syn-rift deposits of the Cretaceous Pigua Subgroup, as expected from regional stratigraphic relationships. The Pigua strata are in turn overlain by the post-rift sediments of the Balbuena and Santa Bárbara subgroups, which have a high signal amplitudes. By extrapolating the imaged units to the surface, they can be clearly seen to be the subsurface equivalents of the west-dipping sedimentary cover rocks of the CR (Figures 1 and 11).

The combination of structural data collected in the field and the results of the analysis of the seismic reflection

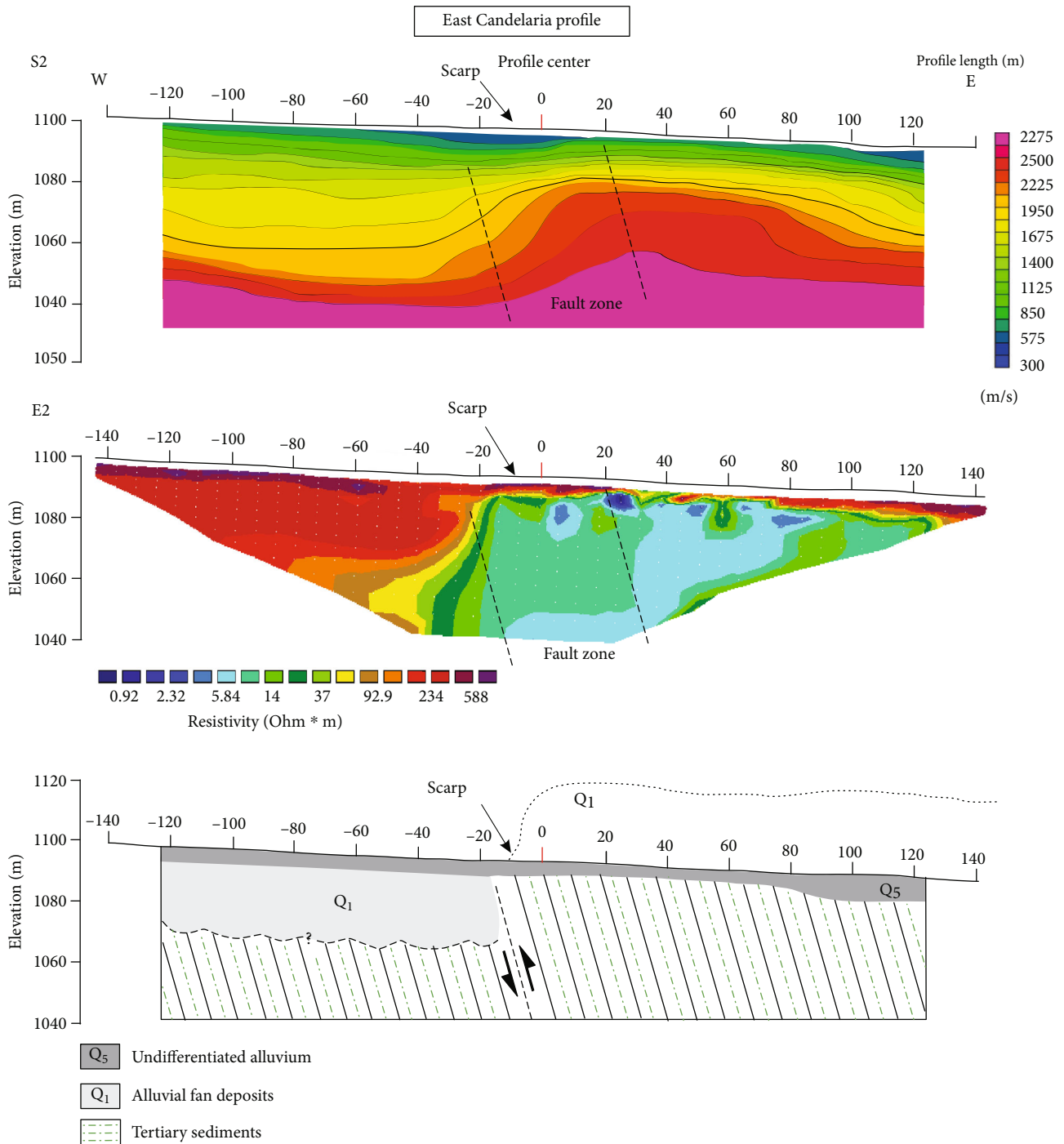


FIGURE 9: Seismic-refraction tomography results for Profile S2 across the East Candelaria fault (see Figure 4(b') for location); seismic velocities are contoured at 275 m/s intervals. Electrical resistivity tomography along Profile E2 (see Figure 4(b') for location). The selected inverse model was obtained after four iterations with an RMS error of 4.2. A dipole-dipole array was used with an electrode spacing of 6 m. Maximum penetration depth was approximately 60 m. Schematic cross-section of profiles E2 and S2, highlighting the fault location and kinematics, is shown at the bottom. This representation shows how the inferred fault generates an upward displacement of the high-velocity layers and coincides with the location of the fault suggested by the electrical resistivity interpretation for Profile E2.

profiles enabled us to model the deformation of the sedimentary cover rocks of the CR using Move2D. First, we attempted to model the deformation in the context of a surface-breaking fault according to the model of Barcelona et al. [24]. In these model runs, the basement rocks exposed

in the range interior would have had to be uplifted 2 km higher compared to their present-day position to generate the folded strata. As we were not able to generate the same flexure on the cover strata as observed in the seismic line with a reactivated fault cutting to the surface, we modeled

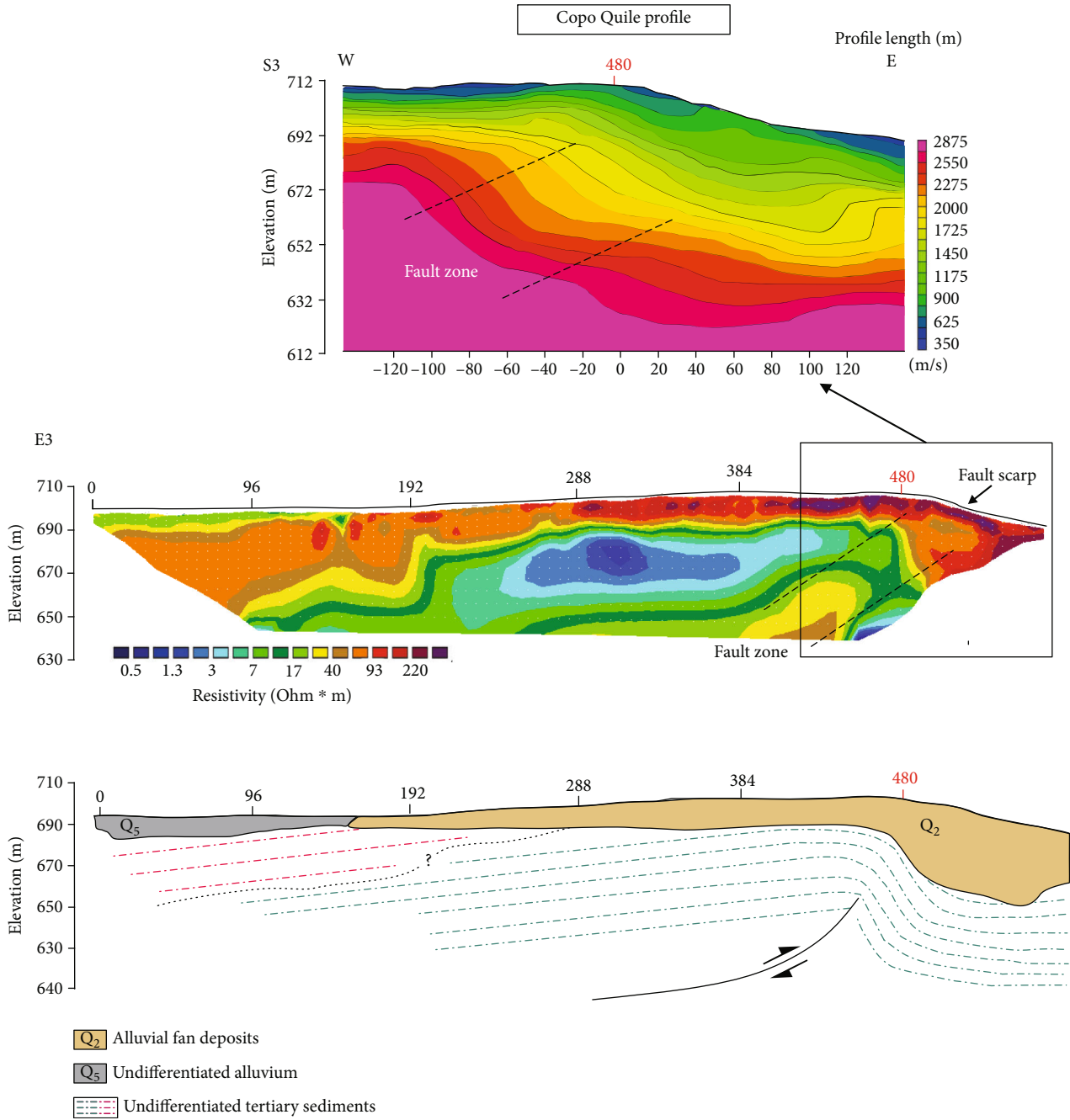


FIGURE 10: Electrical resistivity tomography results for Profile E3 across the Copo Quile fault (see Figure 4(c') for location). The selected inverse model was obtained after two iterations with an RMS error of 7.3. A dipole-dipole array was used with an electrode spacing of 6 m. Maximum penetration depth was approximately 70 m, combining three consecutive profiles. The eastern part of this electrical survey was also investigated with seismic tomography (Profile S3 in Figure 4(c')). Seismic-refraction tomography for S3 results are shown with seismic velocity contours at 275 m/s intervals. Schematic cross-section of Profile E3, highlighting the fault location and kinematics is shown at the bottom. It exhibits how the inferred fault generates an upward displacement of the high-velocity layers; this coincides with the location of the fault suggested by the electrical resistivity interpretation for Profile E3.

the deformation features by introducing a blind fault under the CR, similar to other ranges in the broken foreland (e.g., [2, 34, 82]). Accordingly, by using the Trishear method (i.e., [81]) and by assuming a blind fault under the CR, we were able to generate an asymmetric fold in the sedimentary

cover strata that mimics the field relationships and seismically imaged geometries much better. We therefore conclude that blind faulting underneath the CR is a viable mechanism to explain the deformation of the sedimentary cover rocks of the CR and the Quaternary faulting and warping of the

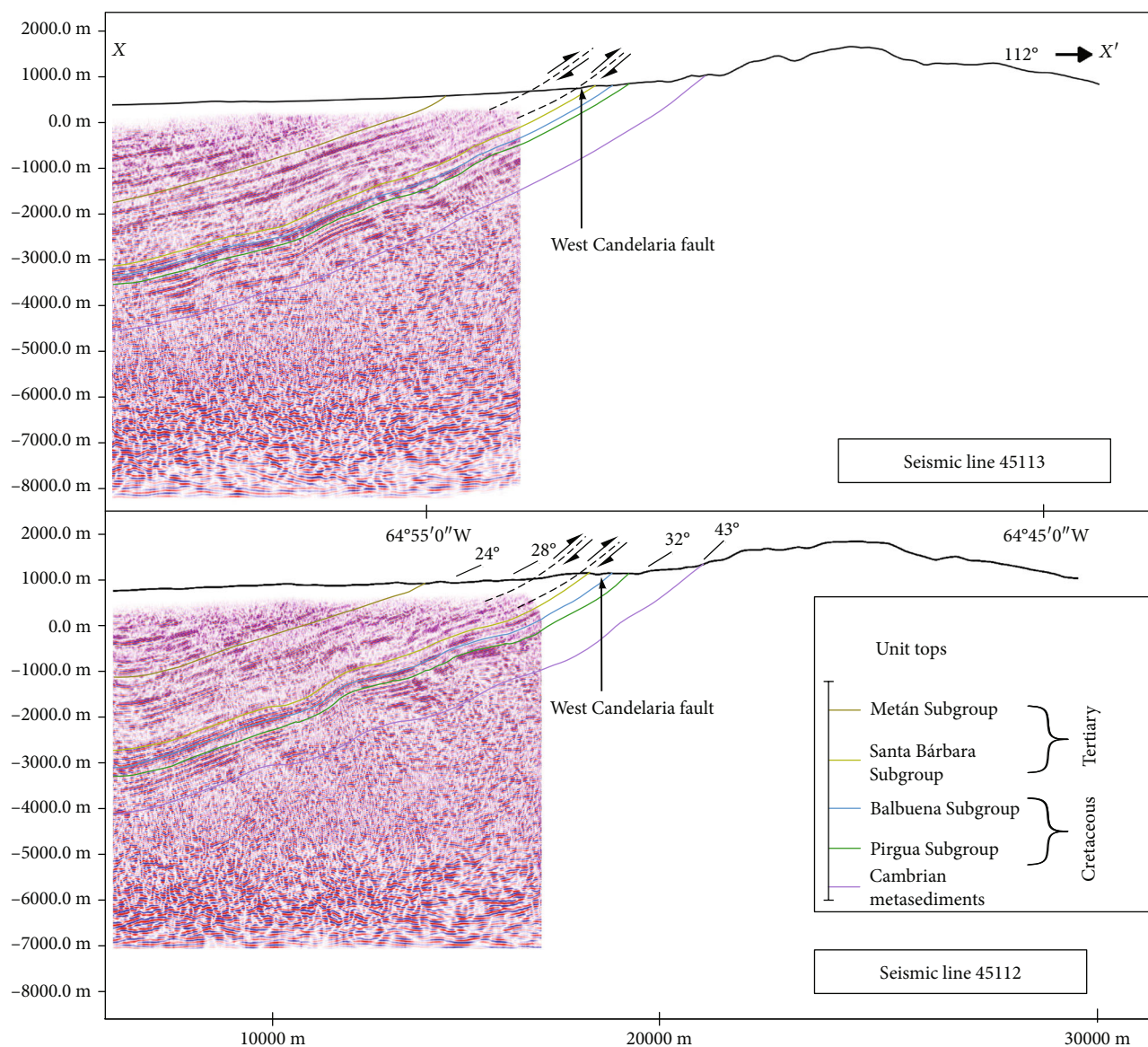


FIGURE 11: Interpretation of the two petroleum-industry seismic reflection lines 45112 and 45113 (see Figure 1 for location), showing the link between outcrops on the western flank of the Candelaria Range and their continuation and geometry at depth as part of flexural-slip deformation. Also shown are stratal dips of the Cretaceous and Tertiary units at surface.

alluvial-fan gravels in the piedmont. Based on the observed relationships, we present a model of the deformation features in Figure 12.

5. Discussion

In Section 5.1, Section 5.2, and Section 5.3, we discuss the characteristics of all three faults identified in the piedmonts of the CR (Figure 1). We review recent structural models in relation to our own field, geomorphic, and geophysical observations and present a simple model for the structural evolution of this foreland sector.

5.1. Morphometric Analysis, Field Observations, ERT and SRT Profiles, and Seismic Reflection Data. Our tectono-geomorphic analysis of the three main faults in the piedmonts of the CR

revealed that spatial variations in topographic gradients within the region are controlled by these three structures. In addition, movement along these faults on both sides of the CR has fundamentally influenced the piedmont fluvial networks, resulting in the development of a trellis drainage pattern. Local uplift along the piedmont faults caused streams to change their flow directions from range-perpendicular to either northward or southward, parallel to the fault scarps. In other cases, sustained incision was able to keep pace with uplift along the piedmont faults, leaving fluvial terraces behind and resulting in the subsequent formation of new alluvial-fan surfaces at successively lower elevations. The gradients of the alluvial-fan terraces are generally greater in the older fan surfaces, suggesting regional uplift and tilting during the growth of the CR. Locally, however, pronounced steps interrupt the longitudinal profiles of the older fan terraces, where we inferred the

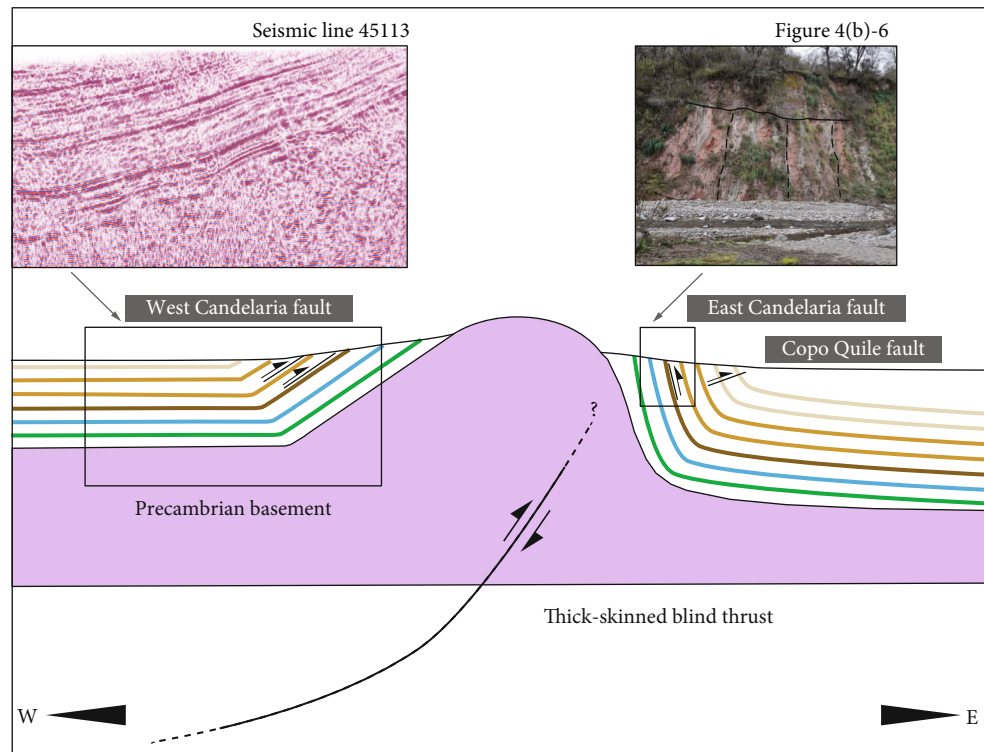


FIGURE 12: Simplified tectonic model of the Candelaria Range with a main blind fault beneath the range, and the West and East Candelaria faults and the Copo Quile fault in both CR piedmonts, showing the folding of the sedimentary cover strata. The model is based on field observations and seismic reflection data analyzed in Move2D.

locations of the piedmont faults. Interestingly, our study did not reveal any evidence of Quaternary activity along a major emergent reverse fault on the eastern range front, nor did we find evidence of any such significant structure bounding the western side of the CR. The basinward dip directions of strata along the flanks of the range and the decreasing inclination of the exposed Cretaceous and Tertiary strata below the western piedmont support these observations (Figure 11). These general characteristics of the gently sloping surfaces only change in the vicinity of the piedmont faults. In light of the warped Cretaceous strata and their contact with unconsolidated Quaternary piedmont gravels along the western flank of the range, the low mountain-front sinuosity index obtained in a remote sensing study by Barcelona et al. [24] is not an indication of tectonic activity. The low sinuosity index may instead reflect the sharp contrast in erodibility between these different lithologies. This scenario is identical to that on the western flank of the Sierra de Quilmes basement uplift in the north-western Sierras Pampeanas (e.g., [82, 83]) and other, asymmetrically uplifted basement blocks in that morphotectonic province (e.g., [2]).

In the western piedmont of the CR, we identified three major scarps (Figure 2), but due to limited accessibility, we focused only on the West Candelaria fault for the geophysical surveys. The models from the two electrical profiles (E1a and E1b; Figures 2, 4, and 8) show low apparent resistivity areas directly beneath the inferred fault scarps, which is consistent with the low resistivity of the shaly strata of the Metán Subgroup sedimentary units. In the northern profile (Profile

E1a), the fault zone has high-resistivity areas that are about 30 m wide on either side (east and west); this is in good agreement with the expected properties (high resistivity) of the alluvial-fan gravels on the western flank of the CR. These gravels comprise metamorphic rocks from basement outcrops that are characterized by high resistivities. The same situation applies to the southern part of the CR along Profile E1b (Figure 8). Profile E1b (Figure 8) also reveals an abrupt horizontal change in resistivity values, which helps to unambiguously determine the location of the West Candelaria fault. Higher seismic velocities that may represent compacted sedimentary strata were vertically translated toward the land surface, which leads to the interpretation of a low-conductivity zone in the model along Profile E1b (Figure 8); in the western part of this profile, the progressive growth of isovelocity layers beneath the inferred fault scarp coincides with the low-resistivity area of the fault zone (Figure 8). The orientation of the fault plane (at -80 to -20 m horizontal distance along the profile) is consequently best explained as representing a west-dipping thrust fault. In the eastern portions of both profiles (E1a and E1b) (Figure 8), the high-velocity and low-resistivity characteristics may relate to shale-rich lithologies. A 25-m-thick layer with relatively high resistivity is interpreted as representing alluvial-fan deposits. At a horizontal distance of 20 m from the center of Profile S1 (Figure 8), the alluvial-fan deposits overlap the fault and form a zone of homogeneous seismic velocities with exceptionally high electrical resistivity. In our interpretation, gravels of metamorphic basement rocks,

together with Cretaceous siltstones and sandstones, were deposited in former river channels along the length of the north-south striking West Candelaria fault and compacted during the Quaternary. The shallow low-resistivity layer on top of the alluvial-fan deposits in Profile E1b (0–50 m) may well be an artifact probably related to a manmade freshwater pond located about 30 m to the north of the profile. The seismic-refraction results for Profile S1 in this area provide more stable, less noisy images of the data obtained from the electrical profiles.

Our two seismic reflection lines from the western CR piedmont allow us to extrapolate the subsurface strata to 7 km depth; the seismic reflection lines also permit us to trace stratal boundaries to the piedmont faults and the tilted outcrops of the sedimentary units that are draped over the CR basement rocks. Importantly, the location of the West Candelaria fault coincides exactly with its up-dip projection from the seismic-reflection stack that corresponds to the sedimentary strata of the Metán Subgroup (Figure 11). No other cross-cutting or steeply dipping faults originating in the basement rocks below can be discerned in the seismic sections. We therefore interpret the West Candelaria fault to be a flexural-slip fault that developed during bed-parallel movement along weak beds within the Neogene sedimentary strata.

On the eastern side of the CR, across the East Candelaria fault, the electrical profiles show high-resistivity values which we interpret as being due to the characteristics of the alluvial-fan deposits (i.e., the high resistivity of the basement-derived conglomerate). This contrasts with the very eastern part of the profile, which presents significantly lower resistivities, possibly reflecting more conductive material such as Tertiary shaly strata. These observations are consistent with the seismic tomography results, which reveal subhorizontal layers with sedimentary characteristics beneath the ground surface, in the upper 40 m of the profile. To the east of the electrical-tomography survey, a marked decrease in resistivity values indicates a change in rock type. This sharp transition in resistivities coincides with the suspected fault location, as well as with the displacement of layers with higher velocities towards the surface in the central part of the seismic tomography profiles (Figure 9). The existence of strata from the Santa Bárbara Subgroup exposed along strike beyond the mapped area to the south (red circle in Figure 1; see photo in Figure 6(b)-6), dipping at 80° toward the east, suggests the presence of a fault. The sharp transition in both resistivity and seismic velocity characteristics also suggests the existence of an east-dipping, high-angle fault, which would best explain this disruption of the alluvial-fan deposits.

Our easternmost geophysical survey in the CR piedmont crosses the north-south striking wedge-like structure that we identified as the Copo Quile fault in the morphological analysis. The high-resistivity layer at the top of the electrical profile (Figure 10, E3), which thickens toward the west, corresponds to alluvial-fan deposits. These units consist of basement-derived conglomeratic gravels, which explains why this top layer is characterized by high resistivity. Below this level, there is a low-resistivity layer approximately 30 m thick, which we interpret as representing a shaly horizon.

This layer has been broken up and uplifted as a result of thrust movements along the Copo Quile fault, cutting through the sedimentary layers at 400 m horizontal distance of profile length, and at elevations of 670 and 650 m (Figure 10, E3). Furthermore, the SRT image reveals a major topographic step, which is similar to the geometry inferred for the other faults (Figure 10, S3). In addition, we observe a vertical change in the velocity gradient and twisted isovelocity lines toward the Copo Quile fault zone. In the ERT profile, the fault zone is characterized by intermediate electrical resistivities values. The results of the ERT and SRT surveys point to the existence of a significant vertical offset in the subsurface layers, which may have forced the development of the wedge-like structure associated with the Copo Quile fault. Moreover, intermediate resistivity values in the westernmost, shallower part of the resistivity model (Figure 10, E3) suggest the existence of unconsolidated sandy or conglomeratic sediments to the west of the wedge-like structure, possibly associated with the youngest phase in the activity of the fault. Growth of this wedge-like structure must have prevented sediments from being transported farther east, resulting in their accumulation behind the wedge.

5.2. Structural Model of the Quaternary Tectonic Evolution of the CR Piedmont Regions. Our structural assessment of the west-dipping West Candelaria fault, the east-dipping East Candelaria fault, and the west-dipping Copo Quile fault (Figure 2) has enabled us to document the Quaternary tectonic activity in the intermontane basins of the central Santa Bárbara morphotectonic province reflected in the deformation of sedimentary cover rocks in the vicinity of the CR. In view of the bed-parallel slip, this deformation must have been forced by deeper-seated processes in the basement rocks that promoted the shortening of the sedimentary strata of the adjacent basins. In contrast to structures in other parts of the Santa Bárbara System and the transition zone between it and the Eastern Cordillera (e.g., [7, 31, 33, 84]), there is no evidence that the West Candelaria fault is a steeply dipping structure which roots into a deep-seated, contractionally reactivated normal fault in the basement. Instead, our detailed field inspections and tectono-geomorphic analyses suggest that the West Candelaria fault is a shallow-rooted surface-breaking structure. In contrast to earlier studies in the western Candelaria piedmont (i.e., [35]), our investigations therefore do not support any model involving a bivergent, pop-up structure that originated in the basement.

In this context, it is important to emphasize that, within the CR, no knickpoints were detected in the longitudinal river profiles that could be associated with the location of the investigated faults, nor were any cataclastic fault zones detected along the flanks of the range. Our knickpoint map (Figure DR2) clearly shows the absence of knickpoints in the transitions between the range and the piedmont areas, where faults had been inferred previously [24]. Furthermore, the Q_1 alluvial-fan deposits overlap the basement rocks of the eastern CR without any interruptions. This setting is reminiscent of the Sierra de Quilmes basement uplift [82, 83] or the Pie de Palo range [34, 85] in the broken foreland of the Sierras Pampeanas farther south (~31°S). By analogy with this style

of deformation and in view of the geomorphic and geological evidence presented herein, we suggest that the uplift of the CR was driven by a major west-dipping blind fault beneath the range, which also resulted in the drape folding of the sedimentary cover rocks. Our modeling of the observed deformational features suggests that blind thrusting under the CR and associated drape folding and warping of strata in the CR and its piedmonts is a realistic model to reconcile the different observations.

In this context, deformation in the intermontane basins may therefore represent second-order, thin-skinned structures that formed during the course of basement-involved deformation and uplift. Accordingly, shortening in the mechanically weak strata of the multilayer Cretaceous rift-fill units and the Cenozoic strata of the intermontane basins on both sides of the CR consequently resulted in flexural-slip thrust faults that broke through to the surface. The cumulative effect of this process was to produce linear fault scarps that are responsible for the formation of the observed trellis drainage patterns and diversions of fluvial channels. This scenario is reminiscent of the evolution of Quaternary flexural-slip faults in areas of flexural-slip folding in the Pamir-western Kunlun and southern Tian Shan regions of Central Asia (e.g., [86, 87]).

Taking into account the results of previous investigations into the Santa Bárbara System and our own new observations and results, we propose that the piedmonts of the broken foreland of the Santa Bárbara System's range uplifts were shaped by a complex, multistage tectonic evolution. The first stage involved extensional processes during the Cretaceous generating normal faults of different scales that bounded a continental graben system [31, 46, 84, 88]. As with other former extensional provinces elsewhere in the Andean foreland (e.g., [89, 90]), these extensional faults were then contractionally inverted during Cenozoic Andean mountain building, resulting in a broken foreland with a spatially and temporally disparate evolution of mountain ranges and intervening basins [4, 7, 23–25, 35, 44]. Sustained shortening, however, also continued to affect the Mesozoic rift-related and Cenozoic syn-orogenic cover rocks in the intermontane basins between the uplifted ranges, resulting in additional basin compartmentalization and interruption of fluvial connectivity and sediment transport toward the undeformed foreland.

5.3. Seismogenic Potential of the Piedmont Faults in the Santa Bárbara System. In our analysis, we have combined the results of a desktop study with field-based geological and geomorphic observations and geophysical evidence across selected piedmont faults of the Candelaria Range, in the broken foreland of the Santa Bárbara System of north-western Argentina. We have been able to show that the intermontane basins of the broken foreland are tectonically active on Quaternary time scales, but we are currently unable to place more definitive bounds on the timing of this activity or to determine whether or not it is indeed associated with seismicity. Small to moderate earthquakes have been recorded within the SBS on decadal time scales by regional [91] and global [92] seismic networks. Damaging earthquakes have also occurred frequently in the past [93, 94].

Macroseismic records from the vicinity of the CR extend back to 1692, when an earthquake with an epicenter to the north of the range and an estimated magnitude of M 7 devastated the settlement of El Esteco [93, 95–98]. Other historical earthquakes in the region occurred in 1826 (Trancas, M 6.5), 1927 (Rosario de la Frontera, M 6.1), and 1931 (El Naranjo, M 6.3) [93, 94, 99]. Damage also occurred in the immediate vicinity of the CR (to the north) during the 2015 Mw 5.8 El Galpón earthquake with a depth of 17 km (Figure 1) [95, 98].

Bearing in mind the modern and historical seismicity in the region, the information on faulting collected during our investigations suggests that the Quaternary fault scarps are an integral part of sustained foreland deformation. However, this style of highly differentiated deformation and the lack of a clear deformation front combine to emphasize the difficulty in efficiently assessing the level of tectonic activity and spatio-temporal trends of potential seismogenic deformation within this morphotectonic province. In the CR piedmont areas, multiple reactivation of the same faults would have been required to generate the pronounced heights of the various scarps (West Candelaria fault: 15 m; East Candelaria fault: 30 m; and Copo Quile fault: 25 m). Alternatively, these scarps could have developed during episodes of aseismic creep, similar to a scenario inferred for active reverse faults in Central Asia (e.g., [100]). In either case, in light of the regional characteristics of seismicity (i.e., [93]), the CR piedmont faults do not appear to have been active very recently (i.e., the last tens to hundreds of years), despite their pronounced morphologic expression, nor has any significant (M >5) seismic activity been recorded recently. There has also been no earthquake damage to infrastructure during the last 150 years. For more advanced future assessment of potential seismogenic hazards associated with the identified faults in the CR piedmonts, it will be necessary to develop a reliable chronology of Quaternary faulting using cosmogenic nuclide dating or optically stimulated luminescence dating of the offset alluvial-fan surfaces, and to define individual surface-rupture events.

Although only qualitative, our assessment of a rather low level of activity on the investigated CR piedmont faults is consistent with the long recurrence interval of strong earthquakes in this region and compatible with the low-strain rates that appear to characterize this sector of the Andean foreland (e.g., [8]). Additional strain-rate data with a higher spatial resolution, as well as additional information on rock types, structural geometries, and topography, will be required for further analysis of the relationships and mechanical coupling effects that could cause earthquake ruptures in this environment of differentially loaded, neighboring faults (e.g., [101, 102]).

6. Conclusions

We used a combination of near-surface geophysical methods, tectono-geomorphic observations, structural field mapping, and morphometric analysis in the Santa Bárbara morphotectonic province of the broken Andean foreland, as a model methodology to derive a comprehensive characterization of fault-rupture zones in an area with recurrent M 7 earthquakes and strong erosional processes. By integrating

geomorphic, geological, and geophysical methods, we have been able to document Quaternary deformation processes in the piedmonts of the Candelaria Range in the Santa Bárbara System that are an integral part of sustained Cenozoic foreland shortening in the north-western Argentinean foreland. Although the high rates of erosion and dense vegetation cover make it difficult to assess active tectonic structures in this environment, our approach has been able to corroborate the presence of prominent morphologic scarps within the alluvial-fan deposits of the Candelaria Range piedmonts that are associated with subsurface flexural-slip fault zones.

On the western piedmont of the Candelaria Range, sharp transitions in electrical resistivity and seismic-refraction data across a 17 km long and 15 m high scarp that has offset and deformed Quaternary alluvial-fan gravels and caused a change in the drainage network, support the interpretation of a fault at depth. Seismic reflection data across this scarp suggest that the observed fault scarp is associated with bedding-plane slip within the Neogene Metán Subgroup strata. The deformation observed suggests that this fault is related to flexural-slip folding in units that have been subjected to protracted folding in a basin between adjacent uplifting and deforming basement ranges. On the basis of our geophysical data and field observations, we suggest a similar origin for the piedmont faults to the east of the Candelaria Range.

The deep-seated processes shaping both piedmont regions are not known at the same level of detail. Nevertheless, the near-surface structure, the orientation, and the overall morphologic character of the identified fault scarps support a model of deformation that involves shortening and flexural-slip folding along rheologically suitable layers in the Mesozoic and Cenozoic sedimentary strata. The broken foreland of the north-western Argentinean Andes thus combines the effects of a thick-skinned deformation style with basement-cored uplifts and the formation of fault scarps related to folding and bed-parallel deformation processes in the intervening basins between these uplifted areas.

In view of the neotectonic deformation style, the typical range of magnitudes for present-day seismicity, and the historical character of seismicity in the broken-foreland region, the heights and lengths of the Quaternary West Candelaria, East Candelaria, and Copo Quile scarps appear to be related to cumulative movement along faults. Repeated offsets during moderate-to-large earthquakes in the Quaternary are the most likely origin for these scarps, which suggests recurrent, spatially disparate seismogenic Quaternary deformation processes in the broken foreland.

Data Availability

The authors confirm that the data supporting the findings of this study are available within the article and its supplementary materials.

Conflicts of Interest

The authors declare that there is no conflict of interest regarding the publication of this article.

Acknowledgments

A. Arnoux was supported by a doctoral fellowship from CONICET, Argentina; the German-Argentinean University Network DAHZ/CUAA (*Riesgos naturales* grant to M. Strecker and A. Gutierrez); and the StRATEGy international training center at Potsdam University, funded by the Deutsche Forschungsgemeinschaft (DFG grant # STR 373/34-1 to M. Strecker). We thank the Secretaría de Minería of Salta Province for the seismic reflection data. We thank R. Alonso, R. Mon, F. Hongn, and G. Aranda for discussions and logistical help.

Supplementary Materials

Supplementary 1. Figure DR1: (A) equipment used in the seismic survey images of the used in the seismic survey; (B) survey design showing location of the source point and the receivers in the three seismic profiles.

Supplementary 2. Figure DR2: drainage map of the Candelaria Range with distribution of Ksn values.

Supplementary 3. Figure DR3: knickpoint map of the Candelaria Range. Knickpoints are represented by circles; the diameter of the circle refers to the offset of the longitudinal profile at the knickpoint location.

References

- [1] T. E. Jordan, B. L. Isacks, R. W. Allmendinger, J. A. Brewer, V. A. Ramos, and C. J. Ando, "Andean tectonics related to geometry of subducted Nazca plate," *Geological Society of America Bulletin*, vol. 94, no. 3, pp. 341–361, 1983.
- [2] T. E. Jordan and R. W. Allmendinger, "The Sierras Pampeanas of Argentina; a modern analogue of Rocky Mountain foreland deformation," *American Journal of Science*, vol. 286, no. 10, pp. 737–764, 1986.
- [3] S. Marshak, K. Karlstrom, and J. M. Timmons, "Inversion of Proterozoic extensional faults: an explanation for the pattern of Laramide and Ancestral Rockies intracratonic deformation, United States," *Geology*, vol. 28, no. 8, pp. 735–738, 2000.
- [4] M. R. Strecker, G. E. Hilley, B. Bookhagen, and E. R. Sobel, "Structural, geomorphic, and depositional characteristics of contiguous and broken foreland basins, examples from the eastern flanks of the central Andes in Bolivia and NW Argentina," in *Tectonics of Sedimentary Basins: Recent Advances*, C. Busby and A. Azor, Eds., pp. 508–521, John Wiley, Chichester, U.K., 2011.
- [5] J. R. Weiss, B. A. Brooks, J. R. Arrowsmith, and G. Vergani, "Spatial and temporal distribution of deformation at the front of the Andean orogenic wedge in southern Bolivia," *Journal of Geophysical Research: Solid Earth*, vol. 120, no. 3, pp. 1909–1931, 2015.
- [6] J. R. Weiss, B. A. Brooks, J. H. Foster et al., "Isolating active orogenic wedge deformation in the southern Subandes of Bolivia," *Journal of Geophysical Research: Solid Earth*, vol. 121, no. 8, pp. 6192–6218, 2016.
- [7] M. P. Hain, M. R. Strecker, B. Bookhagen, R. N. Alonso, H. Pingel, and A. K. Schmitt, "Neogene to Quaternary broken

- foreland formation and sedimentation dynamics in the Andes of NW Argentina (25°S),” *Tectonics*, vol. 30, no. 2, 2011.
- [8] P. K. McFarland, R. A. Bennett, P. Alvarado, and P. G. DeCelles, “Rapid geodetic shortening across the Eastern Cordillera of NW Argentina observed by the Puna-Andes GPS array,” *Journal of Geophysical Research: Solid Earth*, vol. 122, no. 10, pp. 8600–8623, 2017.
- [9] V. A. Ramos, E. O. Cristallini, and D. J. Pérez, “The Pampean flat-slab of the Central Andes,” *Journal of South American Earth Sciences*, vol. 15, no. 1, pp. 59–78, 2002.
- [10] F. González Bonorino, “Algunos problemas geológicos de las Sierras Pampeanas,” *Revista de la Asociación Geológica Argentina*, vol. 5, no. 3, pp. 81–110, 1950.
- [11] R. Mon and J. Salfity, “Tectonic evolution of the Andes of northern Argentina,” *Petroleum Basins of South America: AAPG Memoir*, A. J. Tankard, R. S. Soruco, and H. J. Welsink, Eds., vol. 62, pp. 269–283, 1995.
- [12] J. A. Salfity and R. A. Marquillas, “Tectonic and sedimentary evolution of the Cretaceous-Eocene Salta Group Basin, Argentina,” in *Cretaceous Tectonics of the Andes*, J. A. Salfity, Ed., pp. 266–315, Vieweg, Braunschweig, Wiesbaden, 1994.
- [13] P. England and J. Jackson, “Uncharted seismic risk,” *Nature Geoscience*, vol. 4, no. 6, pp. 348–349, 2011.
- [14] S. Stein, M. Liu, T. Camelbeek et al., “Challenges in assessing seismic hazard in intraplate Europe,” in *Seismicity, Fault Rupture and Earthquake Hazard in Slowly Deforming Regions*, A. Landgraf, S. Kuebler, E. Hintersberger, and S. Stein, Eds., vol. 432 of Geological Society, London, Special Publication, , no. 1pp. 13–28, Geological Society of London, 2017.
- [15] H. Agurto-Detzel, M. Assumpção, M. Bianchi, and M. Pirchiner, “Intraplate seismicity in mid-plate South America: correlations with geophysical lithospheric parameters,” in *Seismicity, Fault Rupture and Earthquake Hazard in Slowly Deforming Regions*, A. Landgraf, S. Kuebler, E. Hintersberger, and S. Stein, Eds., vol. 432 of Geological Society, London, Special Publication, , no. 1pp. 73–90, Geological Society of London, 2017.
- [16] J. R. Arrowsmith, C. J. Crosby, J. Ramo et al., “Surface rupture of the 1911 Kebin (Chon–Kemin) earthquake, Northern Tien Shan, Kyrgyzstan,” in *Seismicity, Fault Rupture and Earthquake Hazard in Slowly Deforming Regions*, A. Landgraf, S. Kuebler, E. Hintersberger, and S. Stein, Eds., vol. 432 of Geological Society, London, Special Publication, , pp. 233–253, Geological Society of London, 2017.
- [17] C. Grützner, R. T. Walker, K. E. Abdрахmatov, A. Mukambaev, A. J. Elliott, and J. R. Elliott, “Active tectonics around Almaty and along the Zailisky Alatau range front,” *Tectonics*, vol. 36, no. 10, pp. 2192–2226, 2017.
- [18] A. Landgraf, S. Kübler, E. Hintersberger, and S. Stein, “Active tectonics, earthquakes and palaeoseismicity in slowly deforming continents,” in *Seismicity, Fault Rupture and Earthquake Hazard in Slowly Deforming Regions*, A. Landgraf, S. Kuebler, E. Hintersberger, and S. Stein, Eds., vol. 432, no. 1, pp. 1–12, Geological Society, London, Special Publication, 2017.
- [19] M. Patyniak, A. Landgraf, A. Dzhumabaeva et al., “Paleoseismic record of three Holocene earthquakes rupturing the Issyk-Ata Fault near Bishkek, North Kyrgyzstan,” *Bulletin of the Seismological Society of America*, vol. 107, no. 6, pp. 2721–2737, 2017.
- [20] E. Calais, A. M. Freed, R. Van Arsdale, and S. Stein, “Triggering of New Madrid seismicity by late-Pleistocene erosion,” *Nature*, vol. 466, no. 7306, pp. 608–611, 2010.
- [21] T. Camelbeek, K. Vanneste, P. Alexandre et al., “Relevance of active faulting and seismicity studies to assessments of long-term earthquake activity and maximum magnitude in intraplate northwest Europe, between the Lower Rhine Embayment and the North Sea,” in *Continental Intraplate Earthquakes: Science, Hazard, and Policy Issues*, vol. 2425, pp. 193–224, Geological Society of America, 2007.
- [22] C. H. Costa, T. Rockwell, J. Paredes, and C. Gardini, “Quaternary deformations and seismic hazard at the Andean orogenic front (31°–33°, Argentina),” in *Fourth International Symposium on Andean Geodynamics, Extended Abstracts*, pp. 187–191, Paris, France, 1999.
- [23] L. D. V. Abascal, “Combined thin-skinned and thick-skinned deformation in the central Andean foreland of northwestern Argentina,” *Journal of South American Earth Sciences*, vol. 19, no. 1, pp. 75–78, 2005.
- [24] H. Barcelona, G. Peri, J. Tobal, L. Sagripanti, and A. Favetto, “Tectonic activity revealed by morphostructural analysis: development of the Sierra de la Candelaria Range, northwestern Argentina,” *Journal of South American Earth Sciences*, vol. 56, pp. 376–395, 2014.
- [25] D. N. Iaffa, F. Sàbat, J. A. Muñoz, R. Mon, and A. A. Gutierrez, “The role of inherited structures in a foreland basin evolution. The Metan Basin in NW Argentina,” *Journal of Structural Geology*, vol. 33, no. 12, pp. 1816–1828, 2011.
- [26] J. A. Salfity, C. R. Monaldi, and O. E. González, *Hoja Geológica 2566-IV Metán, Escala 1:250.000*, Provincia de Salta. Servicio Geológico Minero Argentino 319, Buenos Aires, Escala, 2006.
- [27] S. Kübler, R. Streich, E. Lück, M. Hoffmann, A. M. Friedrich, and M. R. Strecker, “Active faulting in a populated low-strain setting (Lower Rhine Graben, Central Europe) identified by geomorphic, geophysical and geological analysis,” in *Seismicity, Fault Rupture and Earthquake Hazard in Slowly Deforming Regions*, A. Landgraf, S. Kuebler, E. Hintersberger, and S. Stein, Eds., vol. 432 of Geological Society, London, Special Publication, , no. 1pp. 127–146, Geological Society of London, 2017.
- [28] S. Kübler, A. M. Friedrich, R. D. Gold, and M. R. Strecker, “Historical coseismic surface deformation of fluvial gravel deposits, Schafberg fault, Lower Rhine Graben, Germany,” *International Journal of Earth Sciences*, vol. 107, no. 2, pp. 571–585, 2018.
- [29] K. Vanneste, K. Verbeeck, and T. Petermans, “Pseudo-3D imaging of a low-slip-rate, active normal fault using shallow geophysical methods: the Geleen fault in the Belgian Maas River valley,” *Geophysics*, vol. 73, no. 1, pp. B1–B9, 2008.
- [30] P. Alvarado and V. A. Ramos, “Earthquake deformation in the northwestern Sierras Pampeanas of Argentina based on seismic waveform modelling,” *Journal of Geodynamics*, vol. 51, no. 4, pp. 205–218, 2011.
- [31] N. Carrera and J. A. Muñoz, “Thrusting evolution in the southern Cordillera Oriental (northern Argentine Andes): constraints from growth strata,” *Tectonophysics*, vol. 459, no. 1–4, pp. 107–122, 2008.
- [32] V. H. García, F. Hongn, and E. O. Cristallini, “Late Miocene to recent morphotectonic evolution and potential seismic hazard of the northern Lerma valley: clues from Lomas de Medeiros, Cordillera Oriental, NW Argentina,” *Tectonophysics*, vol. 608, pp. 1238–1253, 2013.

- [33] V. H. García, F. Hongn, D. Yagupsky et al., "Late Quaternary tectonics controlled by fault reactivation. Insights from a local transpressional system in the intermontane Lerma valley, Cordillera Oriental, NW Argentina," *Journal of Structural Geology*, vol. 128, article 103875, 2019.
- [34] L. L. Siame, M. Sébrier, O. Bellier et al., "Active basement uplift of Sierra Pie de Palo (Northwestern Argentina): rates and inception from ^{10}Be cosmogenic nuclide concentrations," *Tectonics*, vol. 34, no. 6, pp. 1129–1153, 2015.
- [35] D. N. Iaffa, F. Sàbat, J. A. Muñoz, and N. Carrera, "Basin fragmentation controlled by tectonic inversion and basement uplift in Sierras Pampeanas and Santa Bárbara System, northwest Argentina," in *Thick-Skin-Dominated Orogens: From Initial Inversion to Full Accretion*, M. Nemčok, A. Mora, and J. W. Cosgrove, Eds., vol. 377 of Geological Society, London, Special Publications, , no. 1pp. 101–117, Geological Society of London, 2013.
- [36] R. Gries, "North-south compression of Rocky Mountain foreland structures," in *Rocky Mountain Foreland Basins and Uplifts*, J. D. Lowell, Ed., pp. 9–32, Rocky Mountain Association of Geologists, Denver, Colorado, 1983.
- [37] J. A. Lillegraven, A. W. Snoke, and M. C. McKenna, "Tectonic and paleogeographic implications of late Laramide geologic history in the northeastern corner of Wyoming's Hanna Basin," *Rocky Mountain Geology*, vol. 39, no. 1, pp. 7–64, 2004.
- [38] D. W. Burbank, J. K. McLean, M. Bullen, K. Y. Abdrakhmatov, and M. M. Miller, "Partitioning of intermontane basins by thrust-related folding, Tien Shan, Kyrgyzstan," *Basin Research*, vol. 11, no. 1, pp. 75–92, 2001.
- [39] V. S. Burtman, "Structural geology of variscan Tien Shan, USSR," *American Journal of Science*, vol. 275-A, pp. 157–186, 1975.
- [40] R. W. Allmendinger, V. A. Ramos, T. E. Jordan, M. Palma, and B. L. Isacks, "Paleogeography and Andean structural geometry, northwest Argentina," *Tectonics*, vol. 2, no. 1, pp. 1–16, 1983.
- [41] G. E. Hilley and M. R. Strecker, "Processes of oscillatory basin filling and excavation in a tectonically active orogen: Quebrada del Toro Basin, NW Argentina," *Geological Society of America Bulletin*, vol. 117, no. 7, pp. 887–901, 2005.
- [42] R. Mon, "The structure of the eastern border of the Andes in north-western Argentina," *Geologische Rundschau*, vol. 65, no. 1, pp. 211–222, 1976.
- [43] V. A. Ramos, R. N. Alonso, and M. Strecker, "Estructura y neotectónica de Las Lomas de Olmedo, zona de transición entre los Sistemas Subandino y de Santa Bárbara, Provincia de Salta," *Revista de la Asociación Geológica Argentina*, vol. 61, pp. 579–588, 2006.
- [44] E. Cristallini, A. H. Cominguez, and V. A. Ramos, "Deep structure of the Metan-Guachipas region: tectonic inversion in northwestern Argentina," *Journal of South American Earth Sciences*, vol. 10, no. 5-6, pp. 403–421, 1997.
- [45] J. Kley, C. R. Monaldi, and J. A. Salfity, "Along-strike segmentation of the Andean foreland: causes and consequences," *Tectonophysics*, vol. 301, no. 1-2, pp. 75–94, 1999.
- [46] R. Mon and A. A. Gutiérrez, "Estructura del extremo sur del sistema subandino (provincias de Salta, Santiago del Estero y Tucumán)," *Revista de la Asociación Geológica Argentina*, vol. 62, pp. 62–68, 2007.
- [47] J. H. Reynolds, C. I. Galli, R. M. Hernandez et al., "Middle Miocene tectonic development of the Transition Zone, Salta Province, Northwest Argentina: magnetic stratigraphy from the Metán Subgroup, Sierra de González," *Geological Society of America Bulletin*, vol. 112, no. 11, pp. 1736–1751, 2000.
- [48] M. R. Strecker, R. Alonso, B. Bookhagen et al., "Does the topographic distribution of the central Andean Puna Plateau result from climatic or geodynamic processes?," *Geology*, vol. 37, no. 7, pp. 643–646, 2009.
- [49] P. Baby, P. Rochat, G. Mascle, and G. Hérail, "Neogene shortening contribution to crustal thickening in the back arc of the Central Andes," *Geology*, vol. 25, no. 10, pp. 883–886, 1997.
- [50] B. A. Brooks, M. Bevis, K. Whipple et al., "Orogenic-wedge deformation and potential for great earthquakes in the central Andean backarc," *Nature Geoscience*, vol. 4, no. 6, pp. 380–383, 2011.
- [51] J. F. Dunn, K. G. Hartshorn, and P. W. Hartshorn, "Structural styles and hydrocarbon potential of the sub-Andean thrust belt of southern Bolivia," in *Petroleum Basins of South America*, A. J. Tankard, R. Suarez Soruco, and H. J. Welsink, Eds., vol. 62, pp. 523–543, American Association of Petroleum Geologists, 1995.
- [52] L. Echavarría, R. Hernández, R. Allmendinger, and J. Reynolds, "Subandean thrust and fold belt of northwestern Argentina: geometry and timing of the Andean evolution," *AAPG Bulletin*, vol. 87, no. 6, pp. 965–985, 2003.
- [53] N. McQuarrie, "The kinematic history of the central Andean fold-thrust belt, Bolivia: implications for building a high plateau," *Geological Society of America Bulletin*, vol. 114, no. 8, pp. 950–963, 2002.
- [54] D. Roeder, "Andean-age structure of eastern Cordillera (province of La Paz, Bolivia)," *Tectonics*, vol. 7, no. 1, pp. 23–39, 1988.
- [55] B. M. Sheffels, "Lower bound on the amount of crustal shortening, in the central Bolivian Andes," *Geology*, vol. 18, no. 9, pp. 812–815, 1990.
- [56] C. E. Uba, J. Kley, M. R. Strecker, and A. K. Schmitt, "Unsteady evolution of the Bolivian Subandean thrust belt: the role of enhanced erosion and clastic wedge progradation," *Earth and Planetary Science Letters*, vol. 281, no. 3-4, pp. 134–146, 2009.
- [57] G. E. Bossi, "Geología y estratigrafía del sector sur del Valle de Choromoro," *Acta Geológica Lilloana*, vol. 10, pp. 17–64, 1969.
- [58] V. A. Ramos, "The basement of the Central Andes: the Arequipa and related terranes," *Annual Review of Earth and Planetary Sciences*, vol. 36, no. 1, pp. 289–324, 2008.
- [59] E. C. Moreno, J. G. Viramonte, and J. E. Arias, "Area termal de Rosario de la Frontera y sus posibilidades," *Actas del Segundo Congreso Ibero-Americano de Geología Económica*, vol. 4, pp. 543–548, 1975.
- [60] R. Seggiaro, N. Aguilera, J. Ferretti, and E. Gallardo, "Estructura del área geotérmica de Rosario de la Frontera, Salta, Argentina," *VIII Congreso Geológico Chileno*, vol. 1, pp. 390–394, 1997.
- [61] R. A. Marquillas, C. del Papa, and I. F. Sabino, "Sedimentary aspects and paleoenvironmental evolution of a rift basin: Salta Group (Cretaceous-Paleogene), northwestern Argentina," *International Journal of Earth Sciences*, vol. 94, no. 1, pp. 94–113, 2005.
- [62] F. C. Reyes and J. A. Salfity, "Consideraciones sobre la estratigrafía del Cretácico (Subgrupo Pírgua) del noroeste

- Argentino,” in *V Congreso Geológico Argentino*, pp. 355–385, Asociación Geológica Argentina, Actas III, Buenos Aires, Argentina, 1973.
- [63] J. C. M. Turner, “Estratigrafía del cordón de Escaya y de la sierra de Rinconada (Jujuy),” *Revista de la Asociación Geológica Argentina*, vol. 13, pp. 15–39, 1959.
- [64] J. G. Viramonte, S. M. Kay, R. Becchio, M. Escayola, and I. Novitski, “Cretaceous rift related magmatism in central-western South America,” *Journal of South American Earth Sciences*, vol. 12, no. 2, pp. 109–121, 1999.
- [65] J. A. Gebhard, A. R. Giudici, and J. Oliver Gascón, “Geología de la comarca entre el Río Juramento y arroyo Las Tortugas, provincias de Salta y Jujuy, República Argentina,” *Revista de la Asociación Geológica Argentina*, vol. 29, no. 3, pp. 359–375, 1974.
- [66] C. H. Costa, L. A. Owen, W. R. Ricci, W. J. Johnson, and A. D. Halperin, “Holocene activity and seismogenic capability of intraplate thrusts: insights from the Pampean Ranges, Argentina,” *Tectonophysics*, vol. 737, pp. 57–70, 2018.
- [67] B. Bookhagen and M. R. Strecker, “Orographic barriers, high-resolution TRMM rainfall, and relief variations along the eastern Andes,” *Geophysical Research Letters*, vol. 35, no. 6, 2008.
- [68] F. Castino, B. Bookhagen, and M. R. Strecker, “Rainfall variability and trends of the past six decades (1950–2014) in the subtropical NW Argentine Andes,” *Climate Dynamics*, vol. 48, no. 3–4, pp. 1049–1067, 2017.
- [69] G. I. Marliyani, J. R. Arrowsmith, and K. X. Whipple, “Characterization of slow slip rate faults in humid areas: Cimandiri fault zone, Indonesia,” *Journal of Geophysical Research: Earth Surface*, vol. 121, no. 12, pp. 2287–2308, 2016.
- [70] A. L. Cabrera, *Regiones fitogeográficas Argentinas*, Enciclopedia Argentina de agricultura y jardinería, Acme, Buenos Aires, 1976.
- [71] ASF DAAC, “ALOS PALSAR Radiometric Terrain Corrected Hi res; Includes Material © JAXA/METI 2007,” 2011, November 2017 ASF DAAC.
- [72] W. Schwanghart and N. J. Kuhn, “TopoToolbox: a set of Matlab functions for topographic analysis,” *Environmental Modelling and Software*, vol. 25, no. 6, pp. 770–781, 2010.
- [73] W. Schwanghart and D. Scherler, “Short Communication: TopoToolbox 2 – MATLAB-based software for topographic analysis and modeling in earth surface sciences,” *Earth Surface Dynamics*, vol. 2, no. 1, pp. 1–7, 2014.
- [74] M. H. Loke and R. D. Barker, “Least-squares deconvolution of apparent resistivity pseudosections,” *Geophysics*, vol. 60, no. 6, pp. 1682–1690, 1995.
- [75] M. H. Loke and R. D. Barker, “Rapid least-squares inversion of apparent resistivity pseudosections by a quasi-Newton method,” *Geophysical Prospecting*, vol. 44, no. 1, pp. 131–152, 1996.
- [76] Y. Sasaki, “Resolution of resistivity tomography inferred from numerical simulation,” *Geophysical Prospecting*, vol. 40, no. 4, pp. 453–463, 1992.
- [77] K. Hayashi and T. Takahashi, “High resolution seismic refraction method using surface and borehole data for site characterization of rocks,” *International Journal of Rock Mechanics and Mining Sciences*, vol. 38, no. 6, pp. 807–813, 2001.
- [78] T. J. Moser, “Shortest path calculation of seismic rays,” *Geophysics*, vol. 56, no. 1, pp. 59–67, 1991.
- [79] M. B. Widess, “How thin is a thin bed?,” *Geophysics*, vol. 38, no. 6, pp. 1176–1180, 1973.
- [80] R. Seggiaro, N. Aguilera, J. Ferretti, and E. Gallardo, “Modelo estructural del área termal de la Sierra La Candelaria, departamento Rosario de la Frontera, Salta,” *Revista de la Asociación Geológica Argentina*, vol. 72, no. 6, pp. 265–278, 2015.
- [81] E. A. Erslev, “Trishear fault-propagation folding,” *Geology*, vol. 19, no. 6, pp. 617–620, 1991.
- [82] M. R. Strecker, P. Cerveny, A. L. Bloom, and D. Malizia, “Late Cenozoic tectonism and landscape development in the foreland of the Andes: Northern Sierras Pampeanas (26°–28°S), Argentina,” *Tectonics*, vol. 8, no. 3, pp. 517–534, 1989.
- [83] E. Mortimer, B. Carrapa, I. Coutand et al., “Fragmentation of a foreland basin in response to out-of-sequence basement uplifts and structural reactivation: El Cajon-Campo del Arenal basin, NW Argentina,” *Geological Society of America Bulletin*, vol. 119, no. 5–6, pp. 637–653, 2007.
- [84] N. Carrera, J. A. Muñoz, F. Sábato, R. Mon, and E. Roca, “The role of inversion tectonics in the structure of the Cordillera Oriental (NW Argentinean Andes),” *Journal of Structural Geology*, vol. 28, no. 11, pp. 1921–1932, 2006.
- [85] N. Bellahsen, M. Sébrier, and L. Siame, “Crustal shortening at the Sierra Pie de Palo (Sierras Pampeanas, Argentina): near-surface basement folding and thrusting,” *Geological Magazine*, vol. 153, no. 5–6, pp. 992–1012, 2016.
- [86] T. Li, J. Chen, J. A. Thompson Jobe, and D. W. Burbank, “Active bending-moment faulting: geomorphic expression, controlling conditions, accommodation of fold deformation,” *Tectonics*, vol. 37, no. 8, pp. 2278–2306, 2018.
- [87] J. A. Thompson Jobe, T. Li, J. Chen, D. W. Burbank, and A. Bufe, “Quaternary tectonic evolution of the Pamir-Tian Shan convergence zone, Northwest China,” *Tectonics*, vol. 36, no. 12, pp. 2748–2776, 2017.
- [88] J. Kley and C. R. Monaldi, “Tectonic inversion in the Santa Barbara System of the central Andean foreland thrust belt, northwestern Argentina,” *Tectonics*, vol. 21, no. 6, pp. 11–11–18, 2002.
- [89] A. Mora, M. Parra, M. R. Strecker, A. Kammer, C. Dimaté, and F. Rodríguez, “Cenozoic contractional reactivation of Mesozoic extensional structures in the Eastern Cordillera of Colombia,” *Tectonics*, vol. 25, no. 2, 2006.
- [90] M. Parra, A. Mora, C. Jaramillo et al., “Orogenic wedge advance in the northern Andes: evidence from the Oligocene-Miocene sedimentary record of the Medina Basin, Eastern Cordillera, Colombia,” *Geological Society of America Bulletin*, vol. 121, no. 5–6, pp. 780–800, 2009.
- [91] G. Sanchez, R. Recio, O. Marcuzzi et al., “The Argentinean national network of seismic and strong-motion stations,” *Seismological Research Letters*, vol. 84, no. 5, pp. 729–736, 2013.
- [92] T. Cahill and B. L. Isacks, “Seismicity and shape of the subducted Nazca Plate,” *Journal of Geophysical Research*, vol. 97, no. B12, article 17503, pp. 17503–17529, 1992.
- [93] M. M. Zossi, *Sismicidad y tectónica en los Andes del Norte Argentino, [Ph.D. thesis]*, Universidad Nacional de Tucumán, San Miguel de Tucumán, Argentina, 1979.
- [94] P. Alvarado and M. Araujo, “La importancia de las redes sísmicas locales en la caracterización de la sismicidad cortical más peligrosa de la Argentina,” in *International Conference in Honour of Ing. Alberto Giesecke M*, pp. 57–72, Lima Perú, 2011.
- [95] INPRES, “Instituto Nacional de Prevención Sísmica, Argentina,” 2012, <http://www.inpres.gov.ar>.

- [96] INPRES, “Instituto Nacional de Prevención Sísmica, Argentina,” 2015, <http://www.inpres.gov.ar>.
- [97] INPRES, “Instituto Nacional de Prevención Sísmica, Argentina,” 2019, <http://www.inpres.gov.ar>.
- [98] U. S. Geological Survey, “Earthquake Hazards Program,” 2015, U.S. Geological Survey database <https://earthquake.usgs.gov/earthquakes/eventpage/us10003pc9#executive>.
- [99] L. P. Perucca, A. I. Bracco, and S. M. Moreiras, “Determination of seismogenic structures and earthquake magnitude from seismites in the Acequion River, Precordillera Range, central-western Argentina,” *Journal of Iberian Geology*, vol. 35, pp. 5–18, 2009.
- [100] D. Mackenzie, R. Walker, K. Abdrakhmatov et al., “A creeping intracontinental thrust fault: past and present slip-rates on the northern edge of the Tien Shan, Kazakhstan,” *Geophysical Journal International*, vol. 215, no. 2, pp. 1148–1170, 2018.
- [101] G. E. Hilley, P. M. Blisniuk, and M. R. Strecker, “Mechanics and erosion of basement-cored uplift provinces,” *Journal of Geophysical Research: Solid Earth*, vol. 110, no. B12 article B12409, 2005.
- [102] S. Toda, J. Lin, and R. S. Stein, “Using the 2011 Mw 9.0 off the Pacific coast of Tohoku Earthquake to test the Coulomb stress triggering hypothesis and to calculate faults brought closer to failure,” *Earth, Planets and Space*, vol. 63, no. 7, pp. 725–730, 2011.
- [103] C. Invernizzi, P. P. Pierantoni, A. Chiodi et al., “Preliminary assessment of the geothermal potential of Rosario de la Frontera area (Salta, NW Argentina): insight from hydrogeological, hydro-geochemical and structural investigations,” *Journal of South American Earth Sciences*, vol. 54, pp. 20–36, 2014.